Self- and co-assembly of the amyloid suppressing chaperone DNAJB6b

Carlsson, Andreas

2026

Document Version:
Publisher's PDF, also known as Version of record

Self- and co-assembly of the amyloid suppressing chaperone DNAJB6b

ANDREAS CARLSSON
BIOCHEMISTRY AND STRUCTURAL BIOLOGY | FACULTY OF SCIENCE | LUND UNIVERSITY

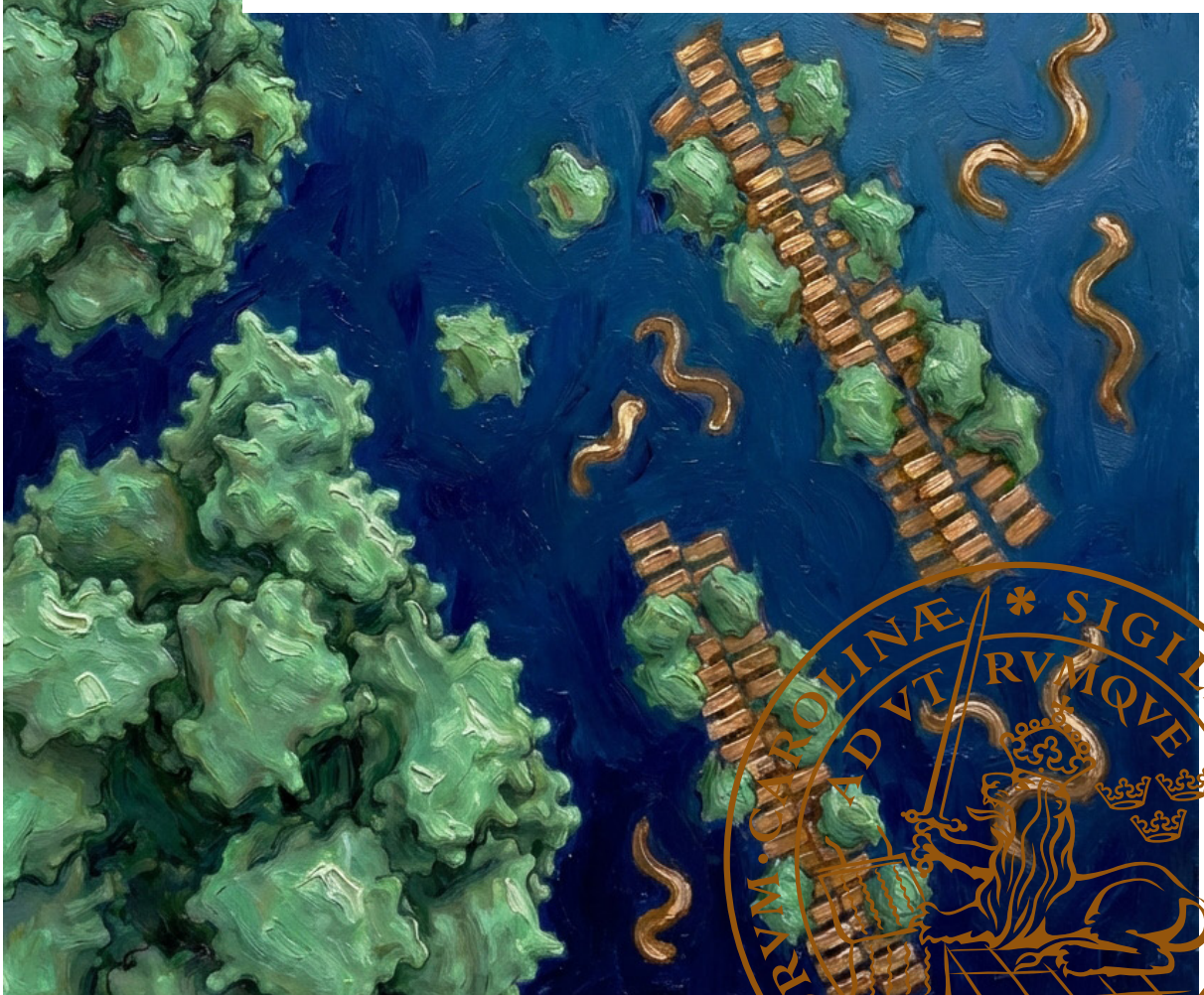

Self- and co-assembly of the amyloid suppressing chaperone DNAJB6b

Self- and co-assembly of the amyloid suppressing chaperone DNAJB6b

by Andreas Carlsson

LUND
UNIVERSITY

Thesis for the degree of Doctor of Philosophy
Thesis advisors: Prof. Sara Linse, Prof. Ingemar Andé, Dr. Thom Leiding
Faculty opponent: Prof. Daniel Otzen

To be presented, with the permission of the Faculty of Science of Lund University, for public criticism in Lecture hall KC:A, Kemicentrum at the department of chemistry on Friday, the 27th of March 2026 at 9:00.

Organization
LUND UNIVERSITY

Biochemistry and Structural Biology
Box 124
SE–221 00 LUND
Sweden

Document name
DOCTORAL DISSERTATION

Date of disputation
2026-03-27

Sponsoring organization

Author(s)
Andreas Carlsson

Title and subtitle
Self- and co-assembly of the amyloid suppressing chaperone DNAJB6b

Abstract

The clustering of certain proteins into oligomers and fibrils, known as amyloids, underlies the pathology of diseases such as Alzheimer's disease, Parkinson's disease, and type 2 diabetes. These processes are counteracted by the cellular protein quality control system, which includes molecular chaperones that interact with disease-associated proteins. One such chaperone is DNAJB6b, which has gained increasing attention over the past decades due to its observed importance in maintaining low levels of harmful protein aggregates.

This thesis aims to deepen our understanding of how DNAJB6b behaves on its own in solution and how it suppresses amyloid formation. The self-assembly of DNAJB6b was investigated under varying solution conditions, revealing that the chaperone readily forms oligomers with a broad size distribution. Monomers are in equilibrium with these oligomers, and the self-assembly resembles that of micelle formation, with an observed critical micelle concentration of approximately 120 nM at room temperature, pH 8.0, and moderate ionic strength. We found that the oligomeric state is virtually inactive in amyloid suppression compared to the dissociated monomeric subunits. We then reversed the perspective and asked which aggregation states of amyloid β are targeted by DNAJB6b. DNAJB6b was found to bind amyloid oligomers with high affinity, likely retarding their conversion into mature fibrils.

Furthermore, the amyloid-suppressive mechanism of DNAJB6b was examined for the amyloid-forming region of the tau protein, which is closely linked to the development of Alzheimer's disease. DNAJB6b exhibited remarkably high inhibition potency, producing a pronounced delay in fibril formation at molar ratios of 1:700 chaperone to tau. Finally, we show that DNAJB6b co-aggregates with tau and binds to tau fibrils, while no detectable interaction with tau monomers was observed.

Together, these insights provide a framework for understanding how DNAJB6b may act as a potent chaperone for amyloid prone proteins. By showcasing the interplay between aggregation states, dynamics, and function, these results may inspire the design of novel therapeutic strategies to counteract protein aggregation in disease.

Key words
chaperones, amyloids, protein aggregation, Alzheimer´s disease, self-assembly, neurodegenerative diseases, DNAJB6b, HSP40, tau, amyloid beta, Aβ42, protein characterization.

Classification system and/or index terms (if any)

Supplementary bibliographical information

Language
English

ISSN and key title

ISBN
978-91-8104-834-6 (print)
978-91-8104-835-3 (pdf)

Recipient's notes

Number of pages
204

Price

Security classification

Self- and co-assembly of the amyloid suppressing chaperone DNAJB6b

by Andreas Carlsson

LUND
UNIVERSITY

.

Cover illustration front:
AI generated image with Google Banana Pro. Illustration of DNAJB6b self- and co-assembly.

Faculty of Science, Biochemistry and Structural Biology

isbn: 978-91-8104-834-6 (print)
isbn: 978-91-8104-835-3 (pdf)

Printed in Sweden by Media-Tryck, Lund University, Lund 2026

Media-Tryck is a Nordic Swan Ecolabel certified provider of printed material. Read more about our environmental work at www.mediatryck.lu.se

MADE IN SWEDEN

Science is like mushroom-picking:
The more careful we are, the less dirt we need to wash away later.
The more knowledge we have, the safer we feel in digesting it.
There is always more to find if we are willing to go searching.
It feels good to have a basket full of it!

- Andreas Carlsson

Contents

List of publications

This thesis is based on the following publications and manuscripts:

i **On the micelle formation of DNAJB6b**

A. Carlsson, U. Olsson, S. Linse
QRB Discovery, 2023, Vol. 4, e6.

ii **The ability of DNAJB6b to suppress amyloid formation depends on the chaperone aggregation state**

A. Carlsson, E. Axell, C. Emanuelsson, U. Olsson, S. Linse
ACS Chemical Neuroscience, 2024, 15(9), pp. 1732-1737

iii **Effects of solution conditions on the self-assembly of the chaperone protein DNAJB6b**

A. Carlsson, V. Maier, C. Fricke, T. Pálmadóttir, I. André, U. Olsson, S. Linse
Communications Chemistry, 2025, 8, 289.

iv **Human chaperone DNAJB6b suppresses tau fibril formation through co-aggregation**

A. Carlsson, E. Axell, J. Wallerstein, D. Thacker, U. Olsson, S. Linse
Submitted manuscript

v **The chaperone DNAJB6b halts amyloid formation through association with transient Aβ oligomers**

J, Gestachew, **A. Carlsson**, E. Axell, D. Thacker, U. Olsson, S. Linse
Manuscript

Publications not included in this thesis:

vi **The C-terminal domain of the antiamyloid chaperone DNAJB6 binds to amyloid-β peptide fibrils and inhibits secondary nucleation**

N. Österlund, R. Frankel, **A. Carlsson**, D. Thacker, M. Karlsson, V. Matus, A. Gräslund, C. Emanuelsson, and S. Linse

Journal of Biological Chemistry, 2023, 299(11)

vii **On the thermal and chemical stability of DNAJB6b and its globular domains**

C. Fricke, J. Milošević, **A. Carlsson**, L. Boyens-Thiele, M. Dubackic, U. Olsson, A. K. Buell, S. Linse

Biophysical Chemistry, 2025, 320-321: 107401

viii **Solubility and Metastability of the Amyloidogenic Core of Tau**

E. Axell, **A. Carlsson**, M. Lindberg, K. Bernfur, E. Sparr and S. Linse

ACS Chemical Neuroscience, 2026

My contributions to the papers

Paper i: I designed and conceptualized the study together with my co-authors. I took part in the purification of DNAJB6b. I performed all MDS experiments and analyzed and plotted all data (both MDS data and the agarose gel electrophoresis results). I wrote the original draft of the manuscript and revised it with input from my co-authors.

Paper ii: I designed and conceptualized the study together with my co-authors. I expressed and purified DNAJB6b. I performed the experimental work, including Aβ42 aggregation kinetics with DNAJB6b, and crosslinking studies to probe the dissociation of DNAJB6b micelles. I wrote the original draft of the manuscript and revised it with input from my co-authors.

Paper iii: I designed and conceptualized the study together with SL and UO. I expressed and purified DNAJB6b and the ΔST mutant and performed or supervised all the experimental work. The experiments I performed include mass photometry, AUC, MDS, refractive index measurements, CD spectroscopy, and HPLC measurements. I wrote the original draft of the manuscript and revised it with input from my co-authors.

Paper iv: I designed and conceptualized the study together with my co-authors. I expressed and purified DNAJB6b, performed the aggregation kinetic studies and fits, conducted the solubility and fibril binding experiments using HPLC, with associated data analysis, provided with samples to cryo-EM and NMR and took part in the measurements. I wrote the original draft of the manuscript and revised it with input from my co-authors.

Paper v: I performed experiments with Aβ42, with MDS and ThT fluorescence to follow the aggregation kinetics. I took part in the experiment design and conceptualization of the MDS experiments. I contributed to the writing of the manuscript.

Populärvetenskaplig sammanfattning

Den här avhandlingen handlar om en del av kroppens försvar mot sjukdomar såsom Alzheimers, Parkinsons, diabetes typ 2, och ALS. Dessa sjukdomar har gemensamt att vissa proteiner i kroppen klumpar ihop sig till långa trådar, kallade *amyloider*, vilket är starkt kopplat till sjukdomarnas förlopp. Amyloider kan bildas i flera delar av kroppen och bestå av många olika typer av proteiner, men vi kommer fokusera på två proteiner som bildar amyloider i hjärnan och då leder till Alzheimers sjukdom. Dessa två proteiner heter *tau* och *amyloid beta*. Tau bildar fibriller inne i nervcellerna och amyloid beta runt om (ofta kallat för plack). Då detta händer skadas nervcellerna. Först tappar de funktion och sedan dör de helt. Detta kallas för neurodegeneration och leder till typiska symptom såsom minnesbesvär och problem med vardagssysslor.

Kroppen har medel för att motverka det spontana bildandet av amyloider. Det finns en typ av proteiner som är specialiserade på att hjälpa andra proteiner att "bete sig korrekt", och passande nog kallas dessa för *chaperoner*, vilket kan översättas till beskyddare på svenska. För att förstå vad jag menar med "bete sig korrekt" måste vi först förstå några grundläggande aspekter av proteiner. Ett protein är uppbyggt av *aminosyror* som är sammanlänkade till en lång kedja. Vi har 20 olika sådana aminosyror som alla har unika egenskaper, såsom storlek, laddning och hur väl de löser sig i vatten. Om dessa aminosyror kedjas efter varandra (vilket händer i kroppen när ett protein tillverkas) så kommer vissa aminosyror vilja vara nära varandra och andra långt ifrån varandra. Detta leder till att proteinet formar sig till en viss struktur, det får en viss *veckning*. Eftersom aminosyrorna kan kombineras i närmast oändlighet så kan en otrolig mängd olika proteiner skapas i kroppen. Vi har runt 10 000 olika proteiner, som alla har sin unika veckning, av evolutionen anpassad för att utföra en viss biologisk uppgift. Men vissa proteiner behöver hjälp med att hitta sin rätta veckning när de skapas, och vissa behöver förhindras att senare felveckas. Det är detta chaperonerna fixar!

Låt oss nu gå tillbaka till de två proteinerna, tau och amyloid beta, som veckar sig felaktigt vid Alzheimers sjukdom och då klumpar ihop sig till toxiska amyloider. Det chaperonprotein som den här avhandlingen handlar om, *DNAJB6* (eller enklare, JB6), förhindrar amyloiderna från att bildas, och därmed håller oss friska. Arbetet i den här avhandlingen handlar om att försöka förstå *hur* JB6 lyckas med sin viktiga uppgift. Genom att undersöka detta väl och lära oss hur JB6 binder till tau och amyloid beta — vilket förhindrar bildandet av amyloider — så kan vi både få en bättre biologisk basförståelse, samt en möjlighet att härma chaperonernas effekt med nya läkemedel mot Alzheimers sjukdom.

Så vilka forskningsframsteg har innehållet i den här avhandlingen bidragit med? För att illustrera detta kan vi använda oss av en liknelse där hjärnan är en skog och Alz-

heimers ett insektsangrepp som långsamt tar död på skogen. I skogen finns ett skyggt djur som på något sätt lyckas hålla skogen frisk. För att förstå hur detta djur gör skulle vi kunna sätta upp övervakningskameror i skogen, och om vi ser att djuret sticker ut en lång tunga och fångar de skadande insekterna så har vi fått ett tydligt svar på vår fråga och skulle kunna gå vidare till nya intressanta frågeställningar.

Det som hindrar oss från att använda ett liknande tillvägagångsätt för att förstå hur JB6 fungerar är att proteiner är så otroligt små — bara några nanometer stora. Det är ungefär så tunt ett hårstrå skulle bli om du klyver dess tjocklek i 10 000 delar. Det är mycket mindre än det synliga ljusets våglängd och därför kan ingen kamera eller ljusmikroskop se så små saker. Vi är därmed tvungna att ta till knep för att lära oss om JB6. Man kan likna det vid att vi försöker mäta allt möjligt på djuret med lång tunga: vi undersöker om det är ett flockdjur, mäter hur mycket det väger, hur snabbt det springer, ser vilka andra djur som finns i närheten, osv. Om vi utan förkunskaper försöker mäta hur mycket djuret ökar i vikt efter en måltid för att förstå vad det äter, kanske vi råkar mäta två djur samtidigt och då felaktigt drar slutsatsen att det äter något som är ungefär lika stort som sig själv. I värsta fall kanske vi inte ens vet om det är rätt djur vi mäter på.

Men om vi har riktigt bra koll på vårt system kan vi lära oss mycket av precisa mätningar. En liten viktökning på djuret när vi systematiskt tillsätter en insekt ger oss en bra indikation på att djuret äter insekter, exempelvis. Det är den här typen av grundläggande undersökningar jag har gjort på JB6. Faktum är att även om proteinerna är så små så kan vi med avancerade tekniker göra mätningar av dess storlek och vikt. Jag har på det här viset insett att JB6 befinner sig ensamt vid låg halt, och bildar ansamlingar på ca 30 st vid högre halter. Dessa större ansamlingar kallar vi för miceller och de verkar fungera som reservoarer som släpper ifrån sig enskilda JB6 molekyler, vilka då kan binda in till amyloiderna och förhindra vidare amyloidtillväxt. Jag har sett att JB6 både kan förhindra amyloidbildning av tau och amyloid beta i provrör, och att JB6 gör detta med en oerhörd effektivitet. Bara en JB6 molekyl per 1000 av amyloid beta eller tau ger en mätbar fördröjning i amyloidtillväxt. Från detta kan vi dra slutsatsen att JB6 binder till små amyloider, innan de blir långa fibriller, och eftersom alla amyloider måste börja små och växa sig stora, så kan JB6 bromsa bildandet i den här flaskhalsen av processen.

Abbreviations

Aβ42	amyloid β 42
AD	Alzheimer's disease
AFM	atomic force microscopy
APR	amyloid prone region
ATP	adenosine triphosphate
AUC	analytical ultracentrifugation
BSA	bovine serum albumin
CD	circular dichroism
cmc	critical micelle concentration
CTD	C-terminal domain
EM	electron microscopy
HPLC	high-performance liquid chromatography
IDP	intrincically disordered protein
IR	infrared
JB6	DNAJB6b
JD	J-domain
k_n	primary nucleation rate constant
k_2	secondary nucleation rate constant
k_+	elongation nucleation rate constant
MDS	microfluidic diffusional sizing
MP	mass photometry
N	aggregation number
NEF	nucleotide exchange factor
NMR	nuclear magnetic resonance
NTD	N-terminal domain
R_H	hydrodynamic radius
SDS PAGE	sodium dodecyl sulfate polyacrylamide gel electrophoresis
$t_{1/2}$	half time of aggregation
ThT	thioflavin T
UV	ultraviolet

Acknowledgements

First and foremost, **Sara** and **Ulf** - you have taught me most of what I know about proteins, molecular interactions, scientific methodology, article writing, supervision and teaching. You are always a source of inspiration to me. A very important aspect that has made me thrive during these years is that you are very kind people. All tasks become so much easier and more fun when I see that you have genuinely fun, and it is obvious that you want me and others to succeed. I will always cherish the times Sara and I have been in the lab and working with different things but still throwing questions and ideas at one another, as well as deep, life-related subjects. I will also always remember the joy which I experienced the Ulf method. For those of you who don't know, he is a thinker and will eventually understand any physical problem presented to him, and in this process he will teach you about the physical world we live in. The perspective you both have given me is priceless. THANK YOU FOR THIS.

To my other supervisors, **Ingemar**: I never started the journey of protein design which we planned that I should do at the start of my PhD, so we unfortunately never worked together as much as planned. However, I am grateful for your help and your enabling of the AUC. **Thom**: We have had many great chats, about everything from lab instruments to communication skills. Thanks for your support!

Emil: So much fun with you! Never a boring time with you in the lab, or on skis, or anywhere really. You bring the energy, the ideas, the creativity, and coffee breaks. I contribute with the boring simple minded "staying-on-the-path mindset", and "let's-finish-what-we-started mindset". Good combo, which has resulted in many joint papers. **Max**: Always the mind I want to pick when thinking about something related to science or life in general (which kind of covers everything for me). And you are always happy to join my weird thoughts. Actually, with the ease you join these thoughts I start to wonder if it is your own thoughts that resonate through me, since you have marinated me with your way of reasoning until I think they are my own… Anyway, a great and generous mind you have! **Ewelina**: I think we did a good job with the students and managed to grab some coffee in between. It is inspiring to see how you take on a PhD education, restoration of a house, and of course, a child. The best of luck to you! **Josef**: Good to have some fellow nano-engineer that sees the world from our (very very small) perspective. It has been fun to see your journey from student to confident scientist. I hope Sanderson will appeal to you! Also, thanks for your efforts with the Abeta-oligomer manuscript when it was close to my printing deadline. **Karolina**: What a great beetroot soup, cat, and husband! Thank you for all food-inspirational lunches and a great time sharing the PhD time. **Elin**: The speed with which you entered the amyloid field impressed me a lot! You contribute always with good energy,

which is so needed during a PhD. **Lei**: I was thought by my parents to always do everything 100 %. But you take the commitment to new heights! Thanks for all fun memories, from drinking wine in the middle of the worst rain Greece had in a century (let's forget the ferry trip home), to proteins getting crosslinked in the dark and fused into One Piece. **Dev**: We have all been spoiled with having Dev in the group. Who would not want to be able to give away a sample and obtain super nice cryo-EM images within short? Almost too convenient… I hope you can teach me soon how to master the frozen art of electron shooting. **Johan**: Lucky me to have a perfect tennis buddy a few rooms away. I am sure we eventually would have found each other, but what were the odds that we meet random at a tennis court and you wanted to warm up a few minutes with me? Then we realized I had just started working in the office next to yours. It is great to chat with you about tennis, life, and science. **Tinna**: The care you show for both scientific methodology and for people is admirable. It will be very interesting to see how the migraine research develops. **Mattias**: Chatting with you is always a pleasure. Your way of seeing humor in the smallest things is inspiring, making me want to pause and speak regardless of the rush in the lab. **Jelica**: Much fun we have had! And you are so nice to speak with about both science and life. I wish you all the best in your endeavors to get better academic conditions in Serbia. **Marija**: Always a good time with you. Many are the times you helped me out of the science bubble and into social mode, which is no easy task! **Rebecca**: Super nice to get to know you in the start of my PhD. You, together with the rest of Sara's group at the time set a very pleasant tone to this group. A smiling, helping, humble tone. **Erik**: A more helpful person is difficult to find. Sometimes you seem like a hundred years old, having had time to experience sooo much! I never stop to marvel at your stories. **Martin**: Thank you for making the lab function well — you are the oil that makes the lab-machinery work. **Jon**: I marvel at the experimental setups you seem to conjure from thin air. You have a lab-solution and a describing theory for everything! **Timas**: Inspiring scientific discussions, I always learn something new!

I cannot understand the luck I have had with the master thesis students I have supervised. Not only have they all been splendid students who curiously (and patiently) learned so much, and produced great work which in all cases have/will lead to publications, they are also very nice colleagues and friends who have been a privilege to work with. You have been a major part in why I have enjoyed going to work during all PhD years. **Celia** was my first student, spoiling me with experience and ideas of an advanced PhD student. Luckily you continue the chaperone research just across Öresund. Then came **Victoria**, who super fast managed to grasp our field and tirelessly obtained high quality data. I hope TUM is treating you with all best! Later, **Lovisa** showed that also LTH can produce the best of students, when you after one meeting with me and Sara came up with splendid scientific questions and pursued your work with ambition and excellent learning skills. Very fun to see that you are staying in the

group! Maybe you will be the one who takes the JB6 project to a satisfying closure (no pressure ;)).

Kalyani: I guess only Sara can rival you when it comes to protein purification. It was great sharing the lab with you! **Tanja**: You are always helpful and friendly, and naturally a great office roomie that makes everyone feel secure and welcome. **Veronica**: Your contagious energy is missed. **Ewa**: Always so nice to meet you when our pathways cross. You bring humanity everywhere you go. **Karin**: When you visit us every year you fill the lab with your warm energy and inspires us all to smile more. **Anders**: We have always inspiring discussions and I appreciate your humble mindset and curiosity. These attributes are so important in science, and I think we all should learn from you. **Alex**: Great to have had you around, both to have a beer with and speculating about chaperone amyloid suppression. **Christin**: Thank you for teaching me how to clean the AUC windows in the best way! **Ajay**: Great to have shared the lab and office with you for several periods of time.

Cecilia: It is fantastic how much literature you have consumed and remember! Thank you for sharing all your knowledge and providing me with a much broader chaperone (and overall biochemical) perspective. Also, I take the opportunity to thank you for laying the foundation to the DNAJB6 field. Without your work I would not have reached a fraction as far in the understanding of this important chaperone, "rescuelin".

Theresa: A person who brightens up every occasion! Which I safely can say based on my empiric study including canoeing, game nights, coffee breaks, hiking, pasta making, badminton, and much else. **Mads**: Nice to have shared the PhD time together, and to host Dora Tang. **Daniel**: When a few coffee cups have been accumulating at my desk, it is always comforting to meet you in the corridor with twice as many ;) **Henrik**: I have always had nice exchanges with you. Thank you for great guidance as institute representative. I have highly appreciated your valuable advises, as well as your anecdotes with coffee or beer in the hand. **Urban**: You taught me in principle all I know about genetics, which I am grateful for. With you, it has always been very nice to take on new students and teach them about Arabidopsis thaliana. **Balder**: The steady pillar to trust in the sometimes stormy sea full of MOBA03 students and PCR questions. **Kristine**: Teaching biophysical chemistry was a good experience with you in the lead. **Carmen**: Finally, after four years alone with the AUC, you decided to join the club! Thanks also for all the experience sharing and enjoyable social occasions — including hosting Dora Tang. **Felipe**: Always so friendly and easy to speak with! I hope your hours spent with a racket in your hand will be many more (which I guess I hope for anyone really…). **Constantinos**: Eventually we will get those noise counts to approach zero! Have faith! **Herwig**: Very good initiative to buy the mass photometer! Thanks for the experience sharing. **Helin**: You set the example of how a good colleague should be — supportive, interested, friendly and welcoming.

Thanks to **everyone else at CMPS** who have made the working climate enjoyable. Keep up the supportive atmosphere! Especially large thanks to the core consisting of **Maryam, Magnus, Tommy,** and **Katja**. You are the essence of the department. Thanks also to all the helpful **colleagues at PhysChem**, who are always open to discussions and collaborations.

Mamma och pappa: Ni har alltid stöttat mig i vad jag tagit mig för. Ni har sett min väg, som inte alls varit solklart inriktad mot en doktorstitel. Trots att det jag gör kan verka långt borta från er vardag så lyckas ni visa stort intresse för allt jag har jobbat med under dessa år. Det har ökat min motivation och dessutom har det hjälpt mig att sätta min forskning i ett större perspektiv när jag pratat med er om vad jag gör. Stort tack för all er stötting och kärlek. Ni är bäst!

Mattias, Elin, Lucas, Alva och Tilda: Ni ger liv till alla tillfällen. Från julfirande och bröllop till Kålmårdsbesök och korvgrillning i Storskogen. Den här lilla boken kanske inte är roligaste kvällsläsningen, men jag misstänker att den kan vara ett utmärkt sömnmedel om ni vill ge det ett försök.

Och sist och störst, tack till dig **Linda**. Det har varit underbart att dela doktorandresan med dig. Du finns alltid där när jag behöver prata av mig, och stöttar mig när det känns svårt. Dessutom har du gett mig mycket hjälpsamma inblickar i både dataanalys och den medicinska forskningsvärlden, samt kommit med superbra feedback på den här avhandlingen. Tack för din förståelse när jag gång på gång missbedömer tiden som labbandet tar. Tänk att vi ändå har lyckats hinna med att både förlova oss och gifta oss under den här tiden! Jag älskar dig.

Chapter 1

Introduction

The aim of this thesis is to deepen our understanding of an important element of the body's natural defense against neurodegenerative diseases such as Alzheimer's and Parkinson's, namely the chaperone protein DNAJB6b (hereafter referred to as JB6).

Several severe diseases have in common that certain proteins aggregate into fibrils, a process closely linked to disease pathology. The most common form of dementia, Alzheimer's disease (AD), is one such condition. In AD, two amyloid-prone peptides — amyloid β and tau — are considered major hallmarks of the disease [1]. These peptides assemble into fibrillar aggregates known as amyloids, which are toxic to neurons and ultimately cause them to lose function and die. Although amyloid formation occurs rapidly *in vitro* at concentrations similar to those found in the body, the disease develops in the time scale of many decades. Hence, the body clearly have endogenous cooping mechanisms to prevent AD. Such mechanisms include chemical degradation, specialized cell types (astrocytes [2] and microglia [3]) and chaperone proteins, sometimes referred to as molecular chaperones [4, 5].

In other words, the body has regulatory systems that maintain a healthy protein balance (proteostasis), but these systems can fail — more frequently with age and in individuals with lifestyle-related risk factors such as smoking or insufficient physical activity [6]. Understanding how these endogenous protective mechanisms work is key to understanding why diseases develops, and may also inspire strategies for designing new medical drugs. One particularly potent amyloid-suppressing chaperone is JB6. About a decade before this thesis work began, JB6 was discovered to play a crucial role in preventing amyloidogenesis in cells [7] and in mice [8]. In vitro studies further showed that JB6 is a strong inhibitor of aggregation by both polyglutamines [9] and the amyloid β peptide (Aβ42) [10]. These promising findings have motivated

further research on JB6, forming a foundation on which the present thesis builds. The choice to study JB6 is further supported by its exceptional potency in suppressing tau accumulation in cells, as demonstrated in a screening study of 50 different chaperones [11] and in comparisons among J-domain proteins (JDPs) [12].

The question of how JB6 functions as a chaperone is complex. It involves both its biological interactions with multiple cellular components and its specific physicochemical interactions with disease-related proteins. Further complicating matters, both the amyloids and JB6 self-assemble into their own different structures, and knowledge of which state interacts with which is needed to study the interplay in detail. By dissecting the problem into smaller pieces which we can learn to understand, we can build the knowledge "bottom up" and hopefully end up with a solid understanding that can be used to fight diseases such as AD.

A major strength of *in vitro* studies, which this thesis work comprises, is that many parameters can be precisely controlled, enabling unknown variables to be isolated and understood. For this reason, **Papers i** and **iii** of this thesis investigate the self-assembly of JB6 in detail. The aggregation of amyloids in the absence of chaperones has already been extensively studied and is not a primary focus here. In **Paper ii**, we examine whether JB6 acts in its oligomeric form or as dissociated subunits. With an understanding of how both the chaperone and the amyloid protein behave independently, as well as which state of JB6 is functionally active, we are finally prepared to address how JB6 prevents the aggregation of the tau protein — a process closely linked to AD pathology. This question is explored in **Paper iv**. In **Paper v**, we probe a binding of JB6 to amyloid oligomers, which are believed to be crucial in AD.

Chapter 2

Background

Proteins

Living organisms consist of many different chemical compounds that work together in intricate ways to build, move, and adapt the organism. Deoxyribonucleic acid (DNA) is commonly referred to as the code of life, whereas proteins can be seen as the workers and building blocks that carry out the mechanisms and processes that make the organism *live*.

Proteins consist of amino acids linked together by covalent peptide bonds into long chains, often hundreds of residues in length. Figure 2.1 illustrates the composition and structure of proteins, from individual atoms to an entire folded protein. When a protein is synthesized in a process called translation, the genetic code is converted into amino acids, providing a blueprint that dictates the order of the building blocks. This order is known as the *primary structure*. Once an amino acid is incorporated into the chain, it is referred to as a residue since a water molecule is released in the process. Human proteins are built from 20 amino acids, each with unique physicochemical properties. These can be categorized in various ways, for example as uncharged, positively or negatively charged, polar or apolar, aromatic, or small versus bulky [13].

The diverse characteristics of the amino acids form the basis for how the peptide chain arranges itself in space [13, 14]. For instance, in a polar environment such as water, hydrophobic residues tend to be buried inside the structure, whereas charged residues must be electrostatically stabilized by opposite charges or electric dipolar moments. The peptide bond has restricted flexibility due to partial double-bond character and steric hindrance [13], meaning that some backbone conformations (dihedral angles) are preferred while others are sterically impossible — commonly visualized in a Ra-

machandran diagram [13]. How the chain twists along its backbone defines the *secondary structure*. The side chains will be arranged to avoid steric clashes, and all hydrogen donors and acceptors need to be hydrogen bonded within the protein or water. Helices and β-sheets are common secondary-structures that satisfy these constraints for certain sequences [13, 15, 16]. How these structures associate in three dimensions defines the *tertiary structure*, often referred to as the fold of the protein. When a part of a protein has a stable fold regardless of the rest of the protein, the part is called a *domain* [13]. When it is not thermodynamically favorable for a protein, or part of a protein, to adopt a stable three-dimensional structure, the result is a highly flexible chain that interacts extensively with the solvent. If this is the case under physiological conditions, the protein is classified as an intrinsically disordered protein (IDP) [17, 18].

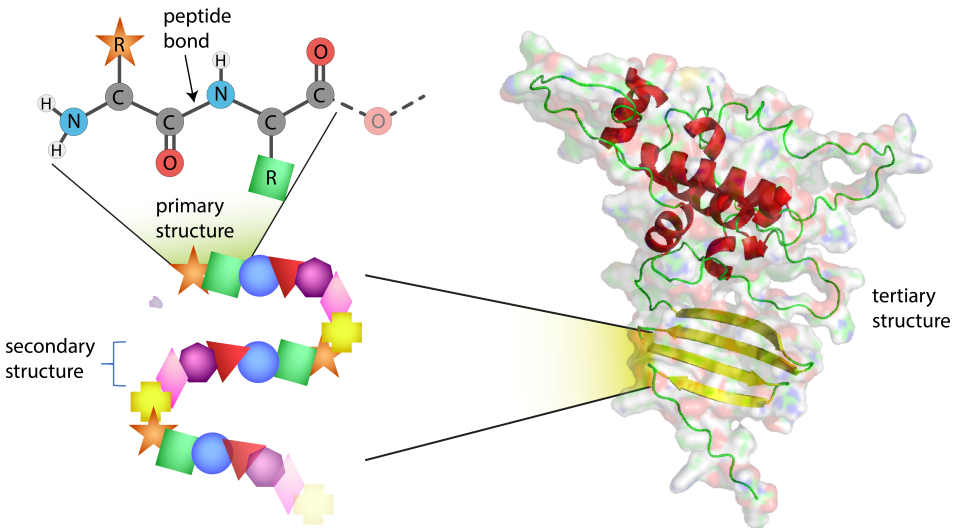

Figure 2.1: The composition and structure of proteins. Two amino acids joined by a peptide bond are shown with all backbone atoms visible and the side chain indicated as an R with a distinct shape to symbolize the diversity of side-chain properties. The sequence order forms the primary structure and the twist of the backbone defines the secondary structure. The fold of the protein as a whole gives the tertiary structure, represented here as an AlphaFold2 structure prediction of DNAJB6b [19, 20], with β-sheets in yellow, helices in red, and the rest in green. The protein surface (determined as the solvent accessible area) is shown semi-transparently, using the software PyMol.

A short chain of coupled amino acids is often referred to as a *peptide*, but it may alternatively be defined as an unfolded amino acid residue chain. In contrast, a protein can be defined as a longer chain, or having a folded structure. There is no strict cut-off between the two terms, and they are sometimes used interchangeably in this thesis.

Protein folding

Both the internal folding of proteins and their association with one another are mainly governed by non-covalent interactions [13]. These interactions depend on the chemical composition and spatial configuration of the polypeptide chain, as well as of the local environment (such as pH, dielectric properties, ionic strength, and temperature). The exception is the disulfide bond between two cysteines, a covalent linkage that can strongly stabilize specific folds [21]. The resulting fold may be more or less well folded or dynamic. Depending on the pathway of folding (sometimes referred to as a folding funnel), these states may reside in a local or global free energy minimum.

The net free energy difference between the folded and unfolded state is a result of large opposing contributions from entropy and enthalpy [14]. The net-resulting protein stability is delicate, and thus, all contributing forces matter for determining the balance between folded and disordered states. While several interactions contribute, the hydrophobic effect is generally regarded as the dominant driving force in protein folding. It arises from the free energy penalty in ordering water molecules around apolar patches of the protein, which promotes the burial of hydrophobic residues within the protein interior [22, 23]. To achieve a well-defined fold, all hydrogen bonds must be satisfied, since the energetic penalty for an unsatisfied hydrogen bond is high, and such conformational states will therefore not be populated to any notable extent [24, 25]. Similarly, isolated ionic groups of the protein will not be buried in a low-dielectric environment, such as hydrophobic parts of the protein, since the electric field of ions need shielding by counter ions and/or molecules with strong electric dipole moments which can order themselves to counteract the electric field [13].

Self-assembly

The phenomenon of molecules that cluster/assemble via non-covalent intermolecular interactions has been studied at least since the early 20th century, as evident from the work of Irving Langmuir in 1916 [26]. These interactions operate at the intersection of chemistry, physics, and biology. What follows in this section is a brief introduction to general aspects of self-assembly, and explanations of some key concepts that will appear throughout this book.

As a start, we categorize different kinds of self-assembly. Depending on the physicochemical and geometrical properties of the molecules in question, as well as solution interactions, they may form *aggregates* in different dimensions, as illustrated in Figure 2.2. In one case, the molecules are stacked on each other in one dimension, forming a linear aggregate, which may be referred to as a fibril or a fiber. This is fairly common in nature and can be related to both biological function and dysfunction/pathology. Disease-related examples include amyloid formation in diseases such as Alzheimer's and Parkinson's (which will be discussed in depth later), and a variant of hemoglobin that causes sickle-cell fiber formation [27]. However, some linear aggregates have biological functions [28], such as storage of peptide hormones [29], antimicrobial activity [30], fertilization [31], bacterial biofilm formation [32], and keratins [33]. On the length scale of a monomer, these structures are virtually infinitely long.

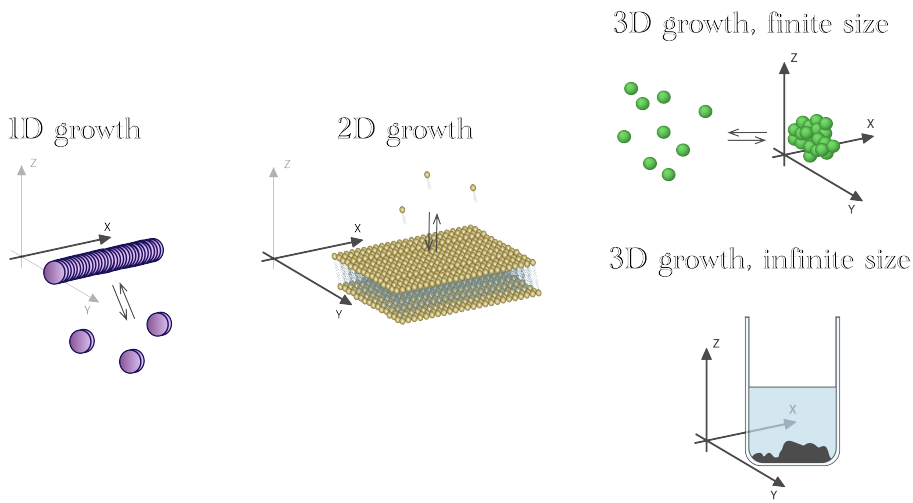

Figure 2.2: Molecules can interact with intermolecular interactions to form aggregates in different orientations, depending on their physicochemical properties and geometry. The schematics show a few examples of how this may be manifested.

In membrane structures, such as the phospholipid membranes that compartmentalize

cells, or in surface adsorption of amphiphilic molecules, the self-assembly is mainly two-dimensional. As with fibrils, the membranes or films can grow to infinite sizes compared to their subunits.

Some molecules — we will focus on proteins in particular — can assemble in three dimensions, forming clusters that can vary greatly in composition, structure, size, and function. In extreme cases, the proteins prefer to exist in an own phase rather than as solutes in the continuous phase, and as a consequence they cluster into infinite aggregates, often amorphous, and "fall out of solution", precipitate. A precipitated protein loses its native structure and function, which is not desired in biology. However, under certain solution conditions, any protein can be soluble, at least to a certain extent. As a solute, a protein will self-assemble in a way that optimizes the free energy of the system, which may differ depending on the protein's physicochemical properties, the solution conditions, and possible co-solutes. The number of molecules that self-assemble into one particle is called the aggregation number, N.

Another important concept is *oligomer*. The term oligomer is used and defined in many different ways, but commonly refers to a self-assembly with an aggregation number higher than one, and low enough that adding or removing a single subunit leads to a "significant difference", according to the IUPAC definition [34]. In this thesis, the term will be used both for intermediate states of amyloid peptides going from monomers to fibrils, and for non-monomeric, soluble forms of other proteins, such as JB6. The fact that these widely different species all can be called oligomers exemplifies how broad the definition is.

Since the oligomerization of JB6 is an equilibrium phenomenon [35], it is useful to call these oligomers *micelles*, defined as colloid-sized aggregates of surface-active molecules that exist in equilibrium with their subunits in solution [36]. Using the law of mass action, and the fact that the chemical potential must be the same for identical molecules in all aggregation states at equilibrium, one can show that micelles are predominantly formed above a critical micelle concentration (cmc), and that the monomer concentration does not increase greatly above this concentration [22]. The exclusion of water from hydrophobic regions drives the self-assembly, and the amphiphilic geometry of the subunits determines the size of the micelles [23]. The concept of protein micelles has been applied before, for instance for α-crystallins [37] and casein [38].

Alzheimer's disease from a molecular perspective

Dementia is a widespread societal challenge and is predicted to be more and more prevalent, mainly due to an increasing population age [39]. Alzheimer's disease (AD) is the most common form of dementia [40], and extensive research has focused on its mechanisms since Alois Alzheimer first characterized the disease in 1907 [41, 42]. In 1984, the extracellular deposits characteristic of AD were identified as aggregates of a peptide later named amyloid β (Aβ) [43]. Despite major research efforts, the biological processes causing AD are still not fully understood. However, the amyloid cascade hypothesis [44, 45] or slightly modified versions of it, is still — after about 35 years since its postulation — the leading hypothesis. The core of the hypothesis is that the disease pathology originates from the extracellular aggregation of amyloid β peptides, forming amyloid fibrils (as described below). Another protein, tau, subsequently aggregates intracellularly, and the disease develops with neurodegeneration and cognitive impairment. The earliest Aβ aggregates typically begin to accumulate 10–30 years before the onset of clinical symptoms [1, 46].

The underlying cause of AD remains debated. Several lifestyle- and health-related factors correlate with an increased risk of developing AD, including traumatic brain injury, obesity, smoking, physical inactivity, and aging itself [6]. However, the levels of amyloid plaque burden and neurofibrillary tangles show direct links to specific genetic variants that substantially increase the risk of AD dementia. These include mutations in the Aβ peptide sequence as well as genetic variations that affect Aβ peptide production, such as those seen in Down syndrome [47] and the Swedish mutant [48].

In recent years, monoclonal antibodies have been designed to bind to Aβ aggregates and provide phagocytosis of the deposits. Lecanemab [49] and donanemab [50] are two such therapeutics which have been approved for clinical use in some regions.

Amyloid-β

Amyloid β peptides are prone to aggregation into extracellular fibrillar assemblies known as *amyloid fibrils*, or simply *amyloids*. These fibrils are defined as stacks of proteins in a β-sheet structure, forming one or more protofilaments that twist around each other along the fibril axis [51]. Amyloid fibrils exhibit a characteristic cross-β X-ray diffraction pattern and typically bind dyes such as Congo red and thioflavin T. The spacing between individual β-strands is approximately 4.7 Å [52].

Extracellular deposits of Aβ fibrils are known as *plaques*. The amyloid β peptides are generated by enzymatic cleavage of the membrane-bound amyloid precursor protein (APP). Depending on the proteolytic processing pathway, peptides of different lengths

are produced, with the most common length being 40 residues (Aβ40). Amyloid β 42 (Aβ42) is the most prevalent one in plaques [47], but also Aβ40 and Aβ43 are frequently found in the fibrils [53]. The sequences of Aβ40-42, and an amyloid structure of Aβ42 are shown in Figure 2.3. The structure is solved for plaque from human brain using cryo-EM microscopy [54], PDB: 7Q4M.

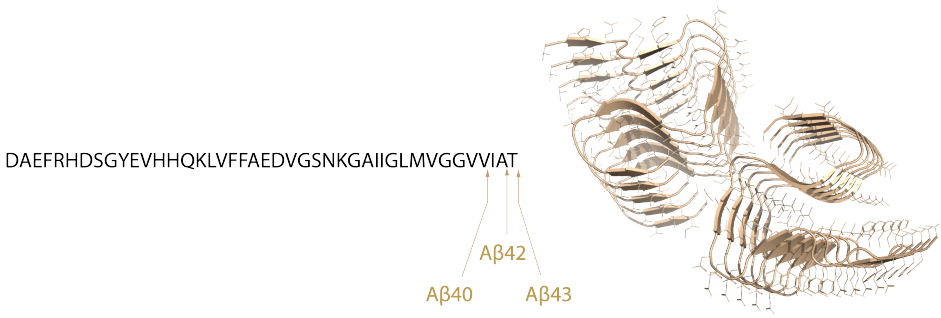

Figure 2.3: Sequence of the Aβ peptide with arrows indicating the ends of Aβ40, 42, and 43. To the right is a fibril structure showing five planes in an Aβ42 fibril, solved from human brain filaments, PDB: 7Q4M. Two protofilaments are twisting around each other.

Tau

The main constitute of neurofibrillary tangles is the tau protein [55]. Alternative splicing of the *MAPT* gene yields six major tau isoforms. Near the N terminus, two segments of 29 and 58 residues may be included or excluded, denoted 1N and 2N. For each of these three N-terminal variants, a 31-residue sequence — repeat region R2 — may or may not be present in the C-terminal half of the protein, giving rise to either three- or four-repeat isoforms (3R or 4R). These repeat regions (R1, R2, R3, R4) mediate tau binding to microtubules [56], a function essential for microtubule assembly [57]. The sequence of the 2N4R isoform (441 residues) is shown in Figure 2.4.

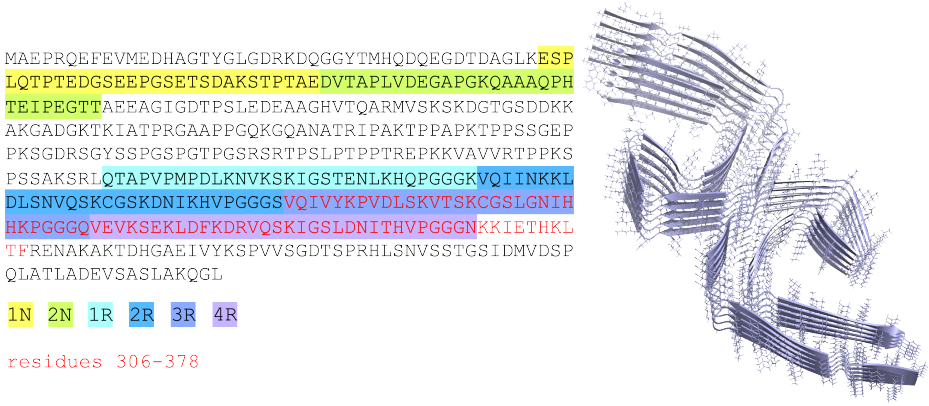

Figure 2.4: Sequence of the 441 residue long tau protein, 2N4R, with color coding as given below the sequence. The residues 306-378 are marked in red, which is the sequence found to compose the fibril core in AD neurofibrillary tangles. Five planes of the (paired helical filament) PHF structure of AD neurofibrillary tangles [58] (PDB: 5O3L) are shown next to the sequence, with two protofilaments in each fibril.

Tau is highly susceptible to phosphorylation [59, 60], and hyperphosphorylation correlates strongly with tau aggregation, likely due to reduced affinity for microtubules [61, 62]. Although tau aggregation occurs in several neurodegenerative disorders [46], this thesis will focus on its role in AD, where tau assembles into amyloid fibrils predominantly of two structural types: paired helical filaments (PHFs) and straight filaments (SFs) [58]. The structured fibril core comprises residues 306–378, while the remaining regions of the protein are less ordered and form a so-called fuzzy coat. A PHF structure consisting of two protofilaments is illustrated in Figure 2.4 [58], with five planes of two protofilaments twisting around each other along the fibril axis.

The fibril core of tau is resistant to proteolytic degradation, resulting in thinner fibrils composed primarily of core residues [63, 64]. Following neuronal death, tau tangles may persist extracellularly as so-called "ghost tangles" [65].

The amyloid-formation process

The assembly of peptides into amyloid fibrils is a well-studied process. Above the solubility limit, nuclei form, which subsequently grow into long fibrils often comprising many thousands of monomers and extending several micrometers in length. This process can be viewed as a phase transition, as there is practically no upper limit to fibril length. The microscopic steps of fibril growth are commonly divided into four steps (Figure 2.5). *Primary nucleation* is the formation of a nucleus whose growth rate exceeds its dissociation rate, resulting in continued growth [66]. *Elongation* describes the addition of monomers to the ends of an existing fibril. An existing fibril surface

can catalyze the formation of new nuclei from monomers of the same type, a process known as *secondary nucleation*. Finally, fibrils may break into two or more fragments, each capable of independent growth, a process termed *fragmentation* [67]. Models that describe the fibril formation with these steps has been established [68, 69] and can be used to obtain the rate constants for the microscopic steps. The free software AmyloFit can be used for this purpose [69].

Both primary and secondary nucleation involve overcoming a free energy barrier to form an elongation-competent species. The transient species are often referred to as *oligomers*. There are several definitions of the amyloid oligomer. Some are related to size and structure, and some are functional definitions with respect to physicochemical and biological properties. The diversity in definitions arises, among other reasons, from heterogeneity in appearance and that they are challenging to study due to low concentrations and transient lifetimes. Nevertheless, oligomers are widely studied due to their central role in disease pathology. They are often considered the most toxic species and are strongly implicated in AD [70, 71, 72, 73, 74, 75, 76]. Oligomeric species also play pathogenic roles in other diseases, such as α-synuclein aggregation in Parkinson's disease [77]. The self-replicating nature of secondary nucleation and fragmentation further contributes to disease progression [78].

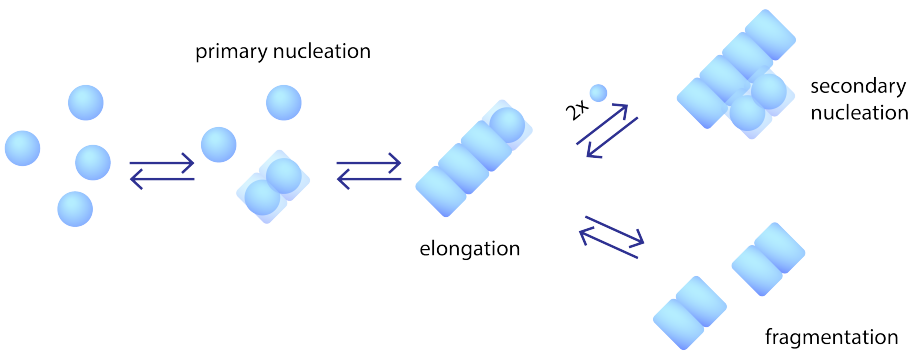

Figure 2.5: Microscopic steps in amyloid formation. Monomers are illustrated as spheres and fibrils as stacked rectangular blocks. The conversion of each monomer into a part of an aggregate is indicated by the superimposed block and sphere.

DNAJB6 — a chaperone protein

A key factor in maintaining a healthy protein balance (proteostasis) can be ascribed to the group of proteins called *chaperones*, or *molecular chaperones*. These proteins function to help other proteins fold correctly and/or prevent them from misfolding and aggregating [79, 4]. The need for chaperones is not surprising given how crowded the cellular environment is — about 20–30 vol-% protein [80] — and about one fourth of the proteome consists of intrinsically disordered proteins [17]. Chaperones are estimated to make up about one tenth of the total protein mass in humans [81], and comprise around 300 different molecular chaperones [5]. Many chaperones are involved in various tasks, taking care of a wide range of *clients*, and are thus often referred to as promiscuous. At the same time, they are specialized to perform certain functions. Some are crucial for the correct folding of newly synthesized proteins by binding to the nascent chain at the ribosome, some are specialized in promoting the degradation of misfolded proteins, and others in refolding them [4].

One of the largest families of chaperones is defined by the presence of a *J-domain*, giving them the name J-domain proteins (JDPs) [82]. This family includes around 50 different chaperones, divided into three subcategories: type A, B, and C [83]. The J-domain is well known to interact with and activate the HSP70 chaperone by forming a complex with nucleotide exchange factors (NEFs) and ATP. The outcome of this activation can vary depending on the situation, but reported consequences include disaggregation, refolding [84], ubiquitylation leading to proteasomal degradation [85], and fragmentation followed by lysosomal degradation [86]. Hence, the JDPs are of particular importance for preventing protein aggregation diseases [87]. Disruption of the chaperone network is one hypothesis for how these diseases arise [5], further emphasizing the need to understand how chaperones operate.

Screening studies to find inhibitors of polyQ peptides [7] and the tau peptide [12, 11] have shown that one of the most effective JDPs in amyloid suppression is *DNAJB6*, which is a non-canonical class B JDP. DNAJB6 is expressed as two isoforms: the 326 residue long a-type and the 241 residue long b-type, sharing 231 residues. Type a is found only in the nucleus, whereas type b is mainly cytosolic [88]. In this thesis, we focus exclusively on type b and refer to this protein as JB6 for simplicity. JB6 is highly expressed in stem cells, but its expression decreases as cells differentiate. This aligns with the observation that amyloids are rarely found in stem cells but are abundant in neurons [89].

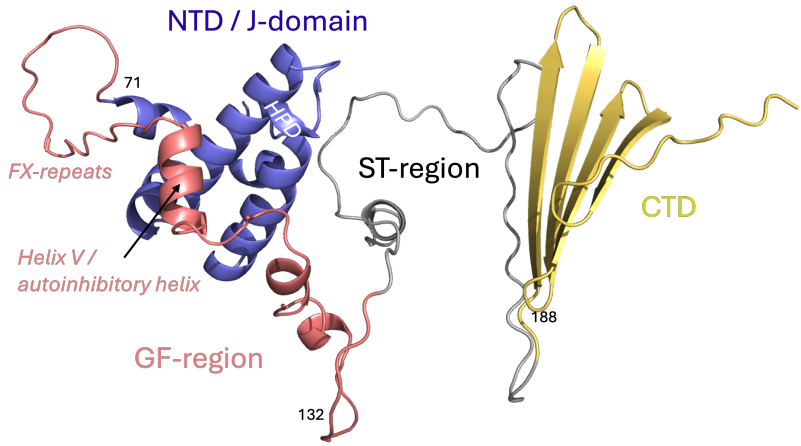

Sequence:
MVDYYEVLGVQRHASPEDIKKAYRKLALKWHPDKNPENKEEAERKFKQVAEAYEVLSDAKK
RDIYDKYGKEGLNGGGGGSHFDSPFEFGFTFRNPDDVFREFFGGRDPFSFDFFEDPFEDF
FGNRRGPRGSRSRGTGSFFSAFSGFPSFGSGFSSFDTGFTSFGSLGHGGLTSFSSTSFGGS
GMGNFKSISTSTKMVNGRKITTKRIVENGQERVEVEEDGQLKSLTINGKEQLLRLDNK

Figure 2.6: AlphaFold2 structure prediction [19, 20] of JB6, colored with the NTD/J-domain in blue, GF-region in red, ST-region in gray, and CTD in yellow.

An AlphaFold2 structure prediction of JB6 is shown in Figure 2.6. The structures of the two folded domains have been experimentally confirmed, and the region between them is predominantly unstructured [90]. The N-terminal domain (NTD) is the J-domain, where the important part of the HSP70 interaction site is the HPD motif. The first half of the linker region is rich in Gly and Phe residues, giving it the name *GF-region*, or *GF-linker*. This part is present (and well conserved) in both the A and B classes of JDPs. In JB6, a short helix (helix V) has been shown to block the HSP70 interaction site when JB6 is not bound to clients, thereby functioning autoinhibitory [90, 91]. The importance of this autoinhibition is evident in mutations causing limb-girdle muscular dystrophy type 1D (LGMDD1), located in the J-domain and in the GF-region near or within helix V. Loss of autoinhibition leads to strong and non-regulated activation of HSP70 [91]. Furthermore, the segment between the J-domain and helix V consists of alternating Phe and other residues (FX-repeats), forming a stretch that stabilizes the interaction with HSP70 [92].

The next part of the linker region is also rich in Gly and Phe, but intermixed with many Ser and Thr residues, giving rise to the name *ST-region*. The function of this part of the linker is less understood in detail, but it is clearly important for client binding [7, 93, 8]. Also the C-terminal domain (CTD) has affinity for amyloid fibrils, and can inhibit secondary nucleation of Aβ42 [94].

It is important to note that JB6 appears to be involved in many cellular processes. It has been identified as a key player in, among other, nuclear pore complex formation [95], keratin turnover [96], and the prevention of myopathy [97, 98]. Its ability to suppress several types of amyloid formation, both as a co-chaperone of HSP70 and independently [82], is summarized in Table 2.1.

Table 2.1: Amyloid-prone peptides whose aggregation is found to be suppressed by JB6.

Peptide / Protein	Associated diseases	References
Amyloid-β peptides	Alzheimer's disease	[10, 93, 99, 100]
Tau	Alzheimer's disease, Pick's disease	[12, 11], Paper iv
α-synuclein	Parkinson's disease, Lewy body dementia, multiple system atrophy	[101, 102, 103, 104]
Polyglutamine peptides (polyQ)	Huntington's disease	[9, 7, 105, 8, 106, 89]
IAPP (islet amyloid polypeptide)	Type 2 diabetes	[107]
TDP-43	Amyotrophic lateral sclerosis (ALS)	[108]

JB6 is also found to inhibit the functional amyloids CsgA and FapC, involved in bacterial biofilm formation [32]. In addition to the vastly different client interactions mentioned above, JB6 displays a strong propensity to self-assemble into polydisperse oligomers [9, 8, 90, 35, 109]. A plausible explanation for this multifaceted interaction behavior is that JB6 has a high chemical potential in solution [110], which it can lower through self- and co-assembly. Most likely, exposed hydrophobic parts of the JB6 linker causes the high chemical potential in aqueous solutions, since water molecules are unfavorably ordered at the hydrophobic surface.

Further description of the self-assembly of JB6 and how it is connected to chaperone activity is the focus of Paper i, ii and iii.

Chapter 3

Methodologies

In this chapter, the most important methodologies used in this thesis work are explained, motivated, and discussed.

Surface adsorption of proteins

Many experiments on protein–protein interactions are most relevant at low protein concentrations (nM to low μM), as these reflect both the physiological concentrations found *in vivo* and the affinities typically involved in such systems. Many proteins are surface active, meaning that they are enriched at surfaces such as the water-air interface or the container of the sample vessel. This leads to a depletion of the protein in solution, lowering the concentration. Since protein concentration is a critical experimental parameter in most studies, the extent of surface adsorption must be evaluated for each protein and surface encountered. Such investigations are sometimes incorporated into the main study, but are often regarded as "base work" and therefore (unfortunately) excluded from publications. Here, I briefly discuss this issue and emphasize its importance for reliable experimental interpretation.

Both amyloid-prone peptides (amyloid β [111] and tau [112]) and the molecular chaperone JB6 [113] are known to be surface active. Consequently, experimental control of their effective concentrations is essential. For instance, when determining the solubility of tau by HPLC with UV absorbance (Paper iv), concentrations in the nM-range were obtained. To confirm that these values reflected the true solubility rather than the fraction remaining after adsorption losses, control experiments were performed. Known concentrations of monomeric tau were subjected to the same sequence of steps as the measured samples — incubation during aggregation, centrifugation in a new tube, and finally a waiting time in a PEG-ylated plate before quantification

with HPLC) — yielding the data shown in Figure 3.1a. Equivalent experiments were conducted for JB6. Surface adsorption proved to be a large issue for JB6 below approximately 100 nM, with complete depletion observed at 15 nM. Tau displayed weaker adsorption, yet at 10 nM the concentration was reduced to roughly half of the initial value.

Similarly, to determine the actual JB6 concentration when examining its affinity for tau fibrils (Paper vi), the protein was quantified by HPLC after incubation in Eppendorf protein low-binding tubes at a volume of 100 µl. These data were used to create an adsorption isotherm (Figure 3.1b), using the inner dimensions of the tubes to estimate the adsorbed amount, Γ. The maximal adsorbed amount per unit area and the affinity towards the surface were obtained by a fit to the Langmuir adsorption isotherm, given in Equation 3.1:

$$\Gamma = \frac{\Gamma_{max} * K * [JB6]_{eq}}{K * [JB6]_{eq} + 1} \tag{3.1}$$

where Γ_{max} is the maximum adsorbed amount and K is the equilibrium constant, with a fitted value of $0.24 * 10^6$ M^{-1}. However, the affinity is likely a lower limit since the aggregation state of JB6 changes with concentration, with larger assemblies at higher concentration that likely increases the adsorbed amount. Indeed, a concentration dependence of the adsorbed amount has been reported for JB6 [113]. This is probably a contributing factor to the higher maximum absorbed amount obtained here (41 mg/m^2) compared to a reported value of 12 mg/m^2 at 0.75 µM JB6 to a silica surface [113]. Furthermore, the roughness of the surface is unknown and may downshift the absorbed amount per unit area further.

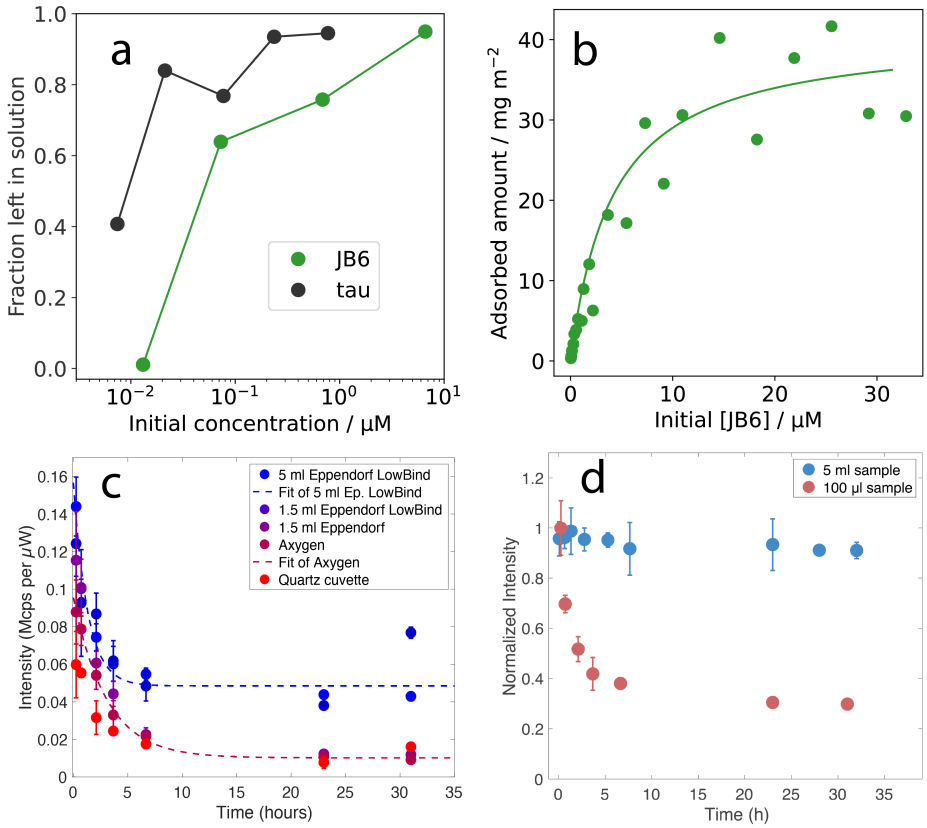

Figure 3.1: Surface adsorption studies. **a**: Quantification of protein remaining in solution after centrifugation and incubation prior to HPLC measurement. **b**: JB6 adsorption to low-binding tubes at a defined surface-to-volume ratio. **c**: Constant surface-to-volume ratio while varying the container material. 20 nM Alexa647-labeled JB6 was quantified by fluorescence intensity using MDS. **d**: Same samples as in c, using Eppendorf protein low-binding tubes and comparing two very different volumes to obtain different surface-to-volume ratios.

Note that the surface materials and volumes are stated above, as both parameters greatly affect how much of the sample adsorbs to surfaces. This is illustrated for JB6 (20 nM Alexa647-labeled) in Figure 3.1c–d, where different container materials were evaluated in panel c, and the effect of varying surface-to-volume ratios is shown in panel d for the Eppendorf low-binding tubes, which performed best among the tested materials. Establishing this information early was essential for drawing relevant conclusions, such as in the cmc determination of JB6 (Paper i) and the dissociation kinetics measured by mass photometry (Paper iii).

Particle sizing

Measuring the size and size distributions of proteins has been central to this work. Understanding the aggregation states of the studied proteins is crucial for interpreting results in chaperone–client systems. Furthermore, the aggregation state is critical when studying the effects of mutations, to identify amino acids involved in a binding site. An interaction between two proteins results from thermodynamic driving forces, and if a mutation weakens the interaction, it is tempting to conclude that the mutated residues are part of the binding site. However, mutations can also alter the protein's fold or self-assembly. In the case of JB6, Paper ii (in combination with insight from Paper iii that the subunit is monomeric) demonstrated that JB6 exhibits substantially higher activity when dissociated into monomers compared to when present as micelles. Consequently, mutations that perturb the micelle–monomer equilibrium or exchange kinetics will inevitably influence the apparent activity of JB6. It is therefore essential to characterize not only the chaperone function, but also the protein's self-assembly and fold, in order to properly interpret the contribution of specific residues to the interaction interface and binding affinities.

Microfluidic diffusional sizing (MDS)

MDS measures the hydrodynamic radius of particles by exploiting diffusion across laminar flow in a microfluidic channel (Figure 3.2). The analyte and buffer flow side by side, and due to Brownian motion, analyte molecules diffuse into the buffer stream. According to the Stokes–Einstein relation, smaller particles diffuse more rapidly:

$$D = \frac{k_B T}{6\pi\eta R_H} \tag{3.2}$$

where D is the translational diffusion coefficient, k_B the Boltzmann constant, T the absolute temperature, and η the solvent viscosity. R_H is the hydrodynamic radius, defined as the corresponding radius of a sphere which yield the same D in Equation 3.2 (given same η and T).

The analyte concentration in each outlet (C_A and C_B) is measured by fluorescence detection, and the fraction that

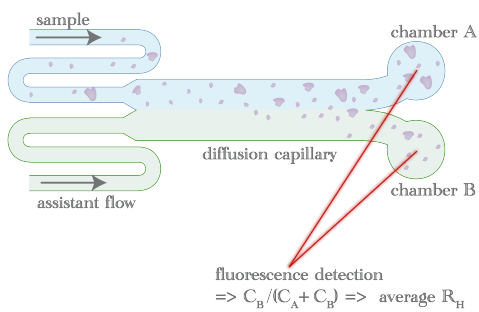

Figure 3.2: Schematic of the microfluidic diffusional sizing (MDS) setup. Based on the R_H of the analyte, diffusion across the laminar flow determines the proportion reaching chamber B. Fluorescence detection quantifies the concentration in each chamber (C_A and C_B), and the diffused fraction, $C_B/(C_A+C_B)$, is used to calculate $\langle R_H \rangle$.

has ended up in chamber B (referred to as the diffused fraction) is used to determine the average hydrodynamic radius, $\langle R_H \rangle$, of the particles [114].

As an example of how much the $\langle R_H \rangle$ can differ depending on solvent interactions and level of folding, bovine serum albumin (BSA) was found to have an $\langle R_H \rangle$ of 3.6 nm when folded and 8.4 nm in as denatured [115]. Since the volume scales with the cube of the radius, the spherical volume upon denaturation corresponds to a 12.7-fold increase in volume.

Mass photometry

This technique, developed in the 2010s [116, 117] is a relatively young technique capable of detecting the masses of individual particles in the range of approximately 40 kDa to 5 MDa [117, 118]. The principle is illustrated in Figure 3.3. A droplet of sample is placed on a glass slide, and a laser beam is reflected off the surface from below. When a particle lands on the surface, the local refractive index changes, leading to a measurable scattering of the laser light. The scattering amplitude is converted to particle mass via a calibration curve, assuming comparable polarizability between the analyte and calibration standards — an assumption that holds for most proteins [117] and was verified for JB6 micelles in Paper iii. The method employs interferometric scattering microscopy [116] to achieve the necessary sensitivity for detecting individual scattering events. After calibration, the resulting output is a mass distribution representing all landing events detected during the measurement period (typically one minute).

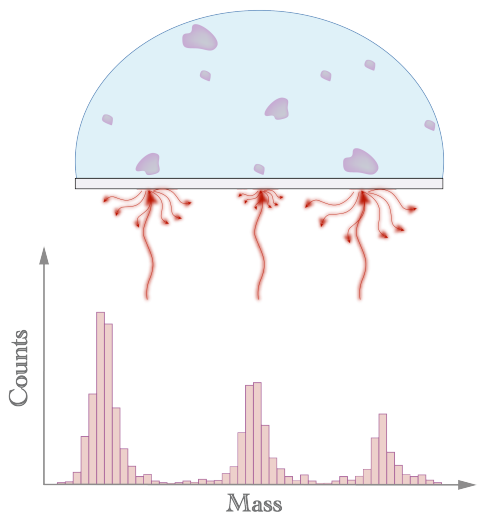

Figure 3.3: Illustration of the principle of mass photometry. Light is scattered to varying degrees depending on the particle masses at the glass surface beneath the sample droplet. The scattering amplitude is converted to mass using a calibration curve, yielding a mass histogram.

Analytical ultracentrifugation (AUC)

AUC has been used to study equilibrium size distributions since its development by Théodor Svedberg in 1923. A detector typically measures absorbance (but it is also pos-

sible with fluorescence or Rayleigh scattering) in a sector-shaped sample cell between two transparent windows during centrifugation. The concentration profile along the radial axis is recorded as a function of time to monitor how fast particles sediment, yielding the sedimentation coefficient S. AUC experiments can be performed in either equilibrium mode, where centrifugal and diffusive forces balance to yield a steady-state distribution, or velocity mode, where the evolution of the sedimentation boundary is analyzed over time [119] (Figure 3.4). The relationship between S, particle mass m_p, and hydrodynamic radius R_H is given by the Svedberg equation:

$$S = \frac{m_{\mathrm{p}} \left(1 - \frac{\rho_{\mathrm{w}}}{\rho_{\mathrm{p}}}\right)}{6\pi\eta R_H} \tag{3.3}$$

where ρ_w is the solvent density and ρ_p the analyte density.

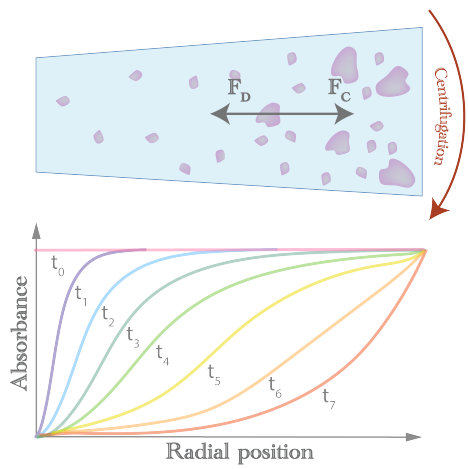

Figure 3.4: Illustration of the analytical ultracentrifugation (AUC) technique. Initially, particles are uniformly distributed within the sector and the absorbance profile is flat. During centrifugation, the particles sediment toward the bottom, altering the absorbance profile. Heavier particles sediment faster, but the frictional drag depends on R_H, meaning that compact particles sediment faster than porous ones.

The output from AUC depends on both particle mass and R_H, which correspond to the parameters obtained from mass photometry and MDS, respectively. These three orthogonal techniques are therefore highly complementary, each reporting on distinct physicochemical properties of the analyte. This complementarity was exploited in Paper iii, where the combined analysis provided insights into the porosity and solvation of JB6 micelles. Furthermore, AUC analyzes the sample in solution, with precise temperature control within 4–40 °C, and the entire sample is included in the analysis. These advantages outweigh its less intuitive output parameter — the sedimentation coefficient. In contrast, the mass photometer provides single-particle mass distributions but has limited temperature control, relies on surface adsorption, and covers a narrower size range.

There are of course many other ways to measure particle size, including static light scattering (SLS), dynamic light scattering (DLS), small angle X-ray light scattering (SAXS), fluorescence correlation spectroscopy (FCS), size exclusion chromatography (SEC), SEC conjugated with multi angle light scattering (SEC-MALS), cryogenic

electron microscopy (cryo-EM), atomic force microscopy (AFM), flow induced dispersion analysis (FIDA), sucrose gradient centrifugation, nano-particle tracking analysis (NTA), and native electrophoresis. Each method has its advantages and disadvantages, making it important to employ several complementary techniques to avoid missing parts of the sample that fall outside a given method's optimal range, or to account for biases toward smaller or larger particles. We therefore chose MDS, mass photometry, and AUC, as they probe different physical parameters and operate over partially overlapping size windows, with the possibility to analyze both non-labeled and fluorescently labeled protein.

Probing aggregation kinetics and solubility

To measure the kinetics of amyloid fibril formation, several different methods can be employed, each with its own advantages and limitations. Depending on the specific system studied, one or more techniques may be suitable.

One of the most commonly used approaches to monitor changes in amyloid mass involves adding an extrinsic fluorophore that exhibits altered quantum yield and/or spectral characteristics upon binding. Thioflavin T (ThT) is one such molecule (Figure 3.5a). ThT binds to amyloid β fibrils with a dissociation constant (K_D) in the sub- to low-μM range [120, 121]. Upon binding, the molecule loses rotational freedom between its two aromatic groups, leading to a pronounced increase in quantum yield [121]. However, the fluorescence response can vary depending on the structure of the bound fibrils — for instance between different morphologies of Aβ40 and Aβ42 [122]. ThT fluorescence was used in Paper ii and v to monitor the increase in fibril mass of Aβ in the presence of JB6.

To study the aggregation kinetics of the tau protein, the dye X34 (Figure 3.5b) is frequently used, owing to its higher quantum yield compared to ThT [123, 124]. This probe was used in Paper iv to monitor aggregation of the amyloidogenic fragment 304–380 of tau.

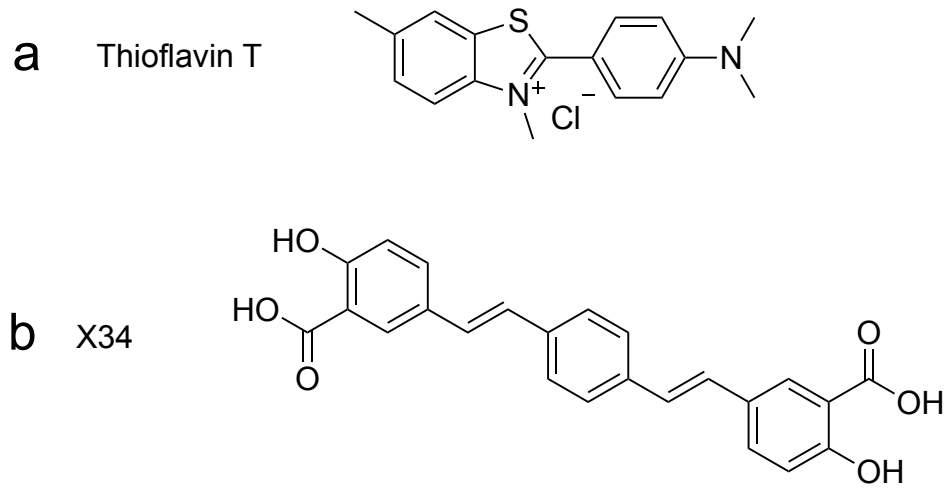

Figure 3.5: Chemical structures of **a**: thioflavin T (ThT), and **b**: X34.

As mentioned above, the quantum yield of these dyes can vary depending on the amyloid structure they bind to, and they are indirect probes of fibril mass. More direct methods include circular dichroism (CD) spectroscopy to monitor spectra of monomers and fibrils, NMR spectroscopy to monitor signals from monomeric species, and protein quantification using, for instance, HPLC, after separation of fibrils from solution (by centrifugation or filtration). The latter approach was employed in Paper iv, confirming that JB6 indeed prolonged the lag phase of tau aggregation, and additionally provided a measure of the tau concentration remaining in solution after aggregation, interpreted as the solubility. A methodological study, focused on obtaining reproducible tau solubility measurements in the low nM-range, was carried out in parallel and resulted in a separate publication [125], not included in this thesis. It may be noted that a true solubility can be reached both from a supersaturated solution and from fibrils alone, with no monomers present in the solution at the start of the experiment. However, a slow dissociation into monomers may provide the latter approach experimentally challenging. Hence, the measured concentration after fibril formation from a supersaturated solution may be referred to as an "apparent solubility", since it may be kinetically trapped in a metastable state.

Chapter 4

Summary of papers

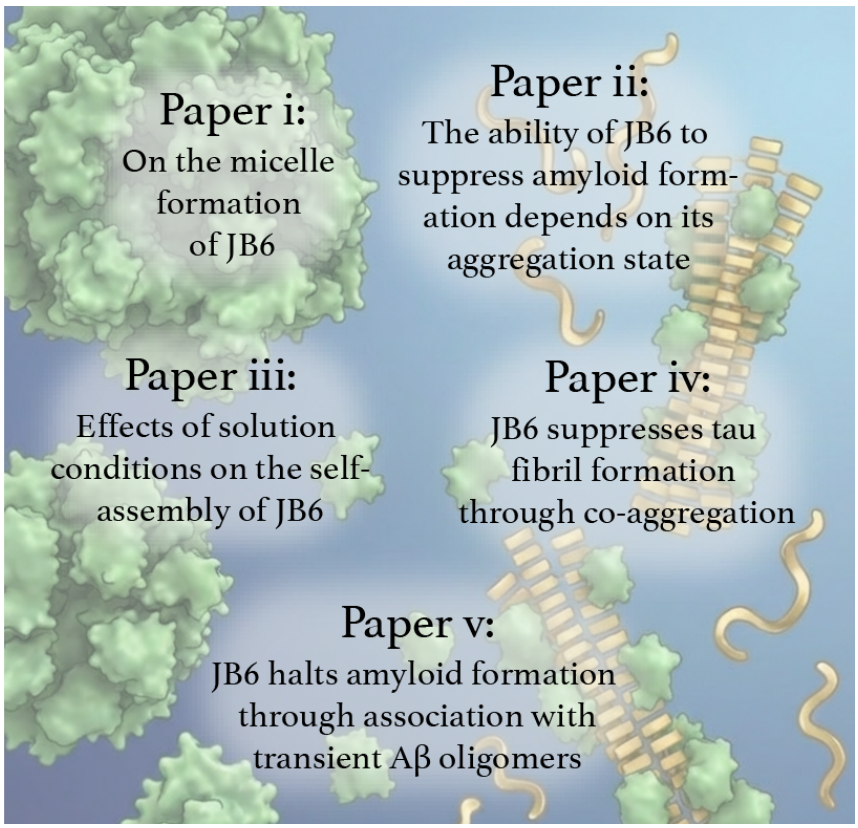

Paper i: On the micelle formation of DNAJB6b

When we initiated this study, we knew it would be the beginning of a long-lasting and extensive project, with the overall goal of understanding why and how JB6 is an effective chaperone. To answer these complex questions, we first needed to establish how JB6 behaves alone. The questions addressed in this article were:

1. How can we probe the self-assembly at low-nM and high-µM JB6 concentrations?
2. Is the observed self-assembly representative of the equilibrium state?
3. How long does it take to reach equilibrium upon dilution?

To address these questions, we conjugated a fluorophore (either Alexa-647 or IR-dye680) to an added cysteine at the C-terminus of JB6. Figure 4.1a shows the fluorophores drawn to scale relative to JB6. To study JB6 at low concentrations, we realized that a large volume-to-surface ratio was necessary to avoid protein depletion from solution due to surface adsorption. This was concluded from the observation that fluorescence intensity decreased in a small volume, but not in a much larger one, as shown in Figure 4.1b.

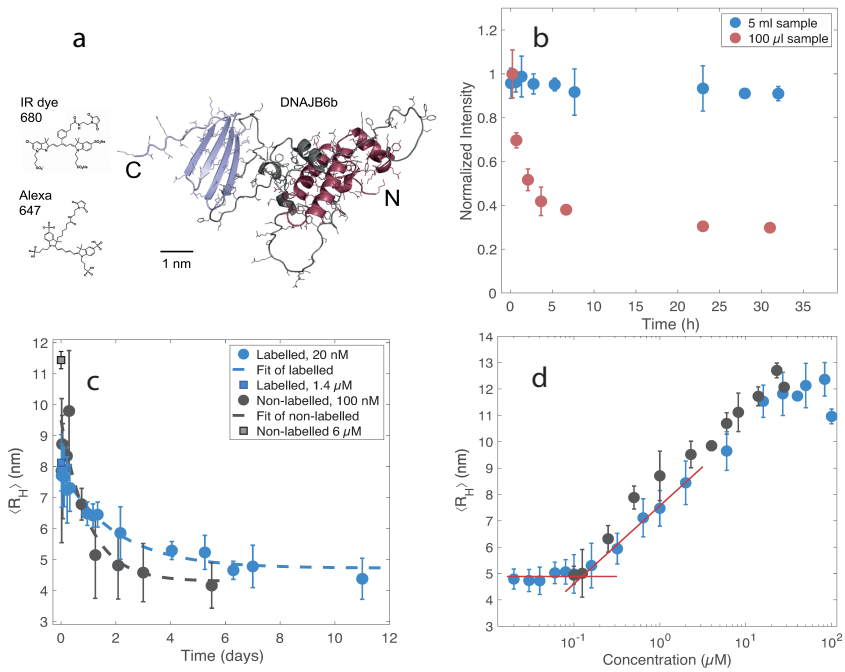

Figure 4.1: **a**: AlphaFold2 structure prediction of JB6 with fluorophores drawn to scale. **b**: The effect of the volume-to-surface ratio when incubating 20 nM Alexa647-JB6 at room temperature. **c**: Using MDS to study the dissociation kinetics of micelles into their subunits. **d**: Concentration dependence of the average R_H at equilibrium. A cmc is found at 120 nM, at room temperature, pH 8.0, and at modest ionic strength.

To measure the time required for JB6 to adapt to a new self-assembly state upon dilution, we followed $\langle R_H \rangle$ as a function of time using microfluidic diffusional sizing (MDS), as shown in Figure 4.1c. We found that dissociation into subunits is a slow process, occurring on the timescale of days at room temperature. We analyzed both Alexa647-labeled and non-labeled JB6 to determine whether the label interfered with the dissociation process. The labeled JB6 dissociated slightly slower, suggesting a minor effect of the fluorophore.

Knowing the equilibration time upon dilution, we prepared a concentration series of JB6, allowed each sample to reach equilibrium, and then measured the dependence of $\langle RH \rangle$ on concentration, as shown in Figure 4.1d. Again, we analyzed both non-labeled JB6 and samples containing 20 nM Alexa647-labeled JB6 mixed with non-labeled protein. Due to technical limitations, the concentration range of non-labeled samples was narrower; nevertheless, we concluded that the label had little or no influence at these stoichiometries. Strikingly, below approximately 100 nM there was no observable concentration dependence of $\langle RH \rangle$, whereas a clear dependence was observed above. This behavior of molecules forming finite-sized assemblies above a more or less critical concentration is consistent with micelle formation. The concept of micelles is therefore useful for JB6 assemblies, as it emphasizes that they are an equilibrium property and can be described by an equilibrium size distribution. The critical micelle concentration (cmc) at room temperature, pH 8.0, and modest ionic strength was determined to be approximately 120 nM.

To complement the MDS experiments, native agarose gel electrophoresis [126] was performed using a concentration series of JB6 spiked with 5 nM IR-dye680-labeled JB6 (Figure 4.2). A transition to lower electrophoretic mobility was observed between 69 and 131 nM, in agreement with the cmc of 120 nM obtained by MDS.

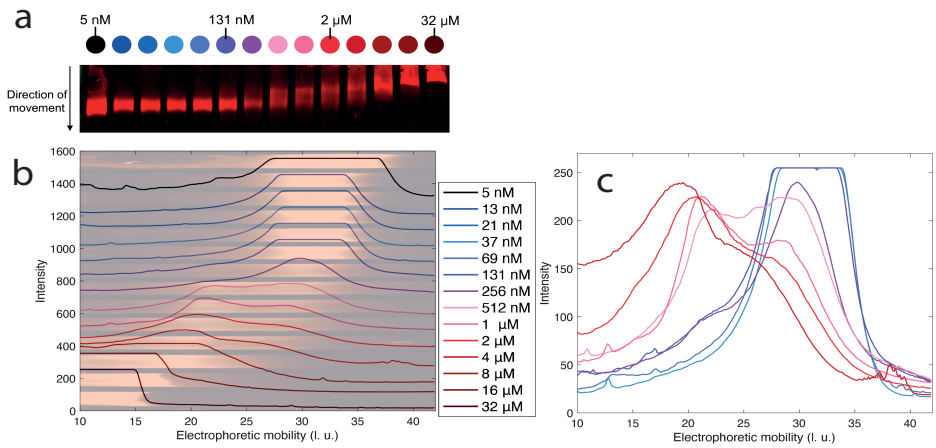

Figure 4.2: Native agarose gel electrophoresis of different JB6 concentrations, with IR-dye-labeled JB6 as probe. **a**: IR-fluorescence scan of the blotted gel. **b**: Electrophoretic mobility profiles superimposed with the corresponding gel scan. **c**: Profiles around the cmc plotted on a common y-axis.

Paper ii: The ability of DNAJB6b to suppress amyloid formation depends on the chaperone aggregation state

In this work, we aim to answer the question: "Are the JB6 micelles or their subunits the active species in amyloid inhibition?"

It is in principle a simple question. However, we wanted to obtain experimental evidence using non-modified proteins — that is, without mutations, fluorophore labeling, crosslinking, or other chemical modifications. Otherwise, we would only obtain an indicative answer. To achieve this, we took advantage of the slow dissociation kinetics of JB6 upon dilution, identified in Paper i, by adding JB6 at different stages of dissociation to monomeric Aβ42 and observing whether the inhibitory activity depended on the aggregation state of JB6. The methodology is illustrated in Figure 4.3.

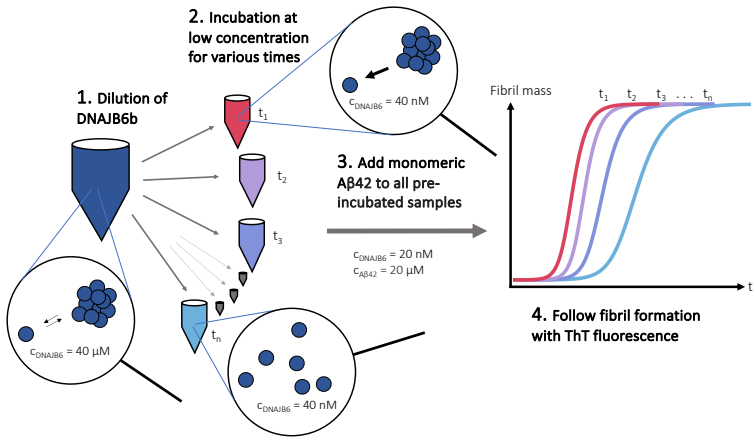

Figure 4.3: Experimental setup. JB6 was diluted 1000-fold (to below the cmc) and incubated for various times. Monomeric Aβ42 was then added to all samples, and ThT fluorescence was used to follow fibril formation.

The kinetic traces are shown in Figure 4.4. A clear trend is observed: JB6 becomes a more potent amyloid inhibitor the longer time it has had to dissociate. To compare the inhibition efficiency with the aggregation state of JB6, the half-times ($t_{1/2}$) of each kinetic trace and the corresponding $\langle R_H \rangle$ values were plotted versus the time since JB6 dilution (Figure 4.5). The dissociation process and increase in $t_{1/2}$ follow each other well. We therefore conclude that JB6 must dissociate into its subunits to become fully active. Since this conclusion relies on the dissociation kinetics previously measured by MDS, we complemented those data with an orthogonal method: chemical crosslinking followed by aggregation-state quantification using SDS-PAGE, which confirmed that dissociation at room temperature occurs on the timescale of days.

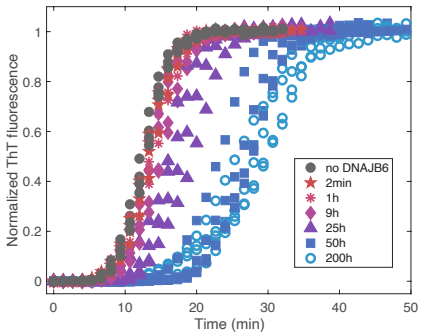

Figure 4.4: Aggregation kinetics of 20 μM Aβ42 in the presence of 20 nM JB6, which was pre-equilibrated for differently long times, to obtain JB6 at various stages of dissociation: from micelles at short times to fully dissociated subunits at long times.

The $\langle R_H \rangle$ is not a reliable measure for determining whether JB6 is predominantly monomeric, dimeric, or composed of a mixture of species, which is why we here refer to the dissociated form simply as "subunits." Later, in Paper iii, we will discover that these subunits are monomers.

It can be noted that an unusually high concentration of Aβ42 (20 μM) was used. This was necessary in order to achieve a short lag phase (<10 min), thereby preventing JB6 dissociation during the fibril formation process, which was conducted at 37 °C. At this stage, we hypothesized that the reason for this was that the micelles dissociate much faster at 37 °C. Later, in Paper iii, we will find this to be the case.

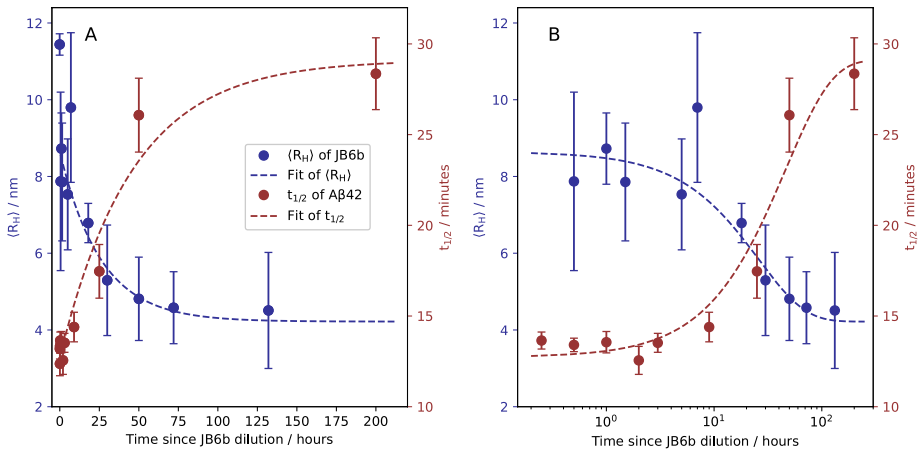

Figure 4.5: Comparison of the JB6 micelle dissociation kinetics (blue, left y-axis) and the Aβ42 fibril formation half-time (red, right y-axis) as a function of JB6 pre-incubation time. A fit to the $t_{1/2}$ data, in the form $t_{1/2}(t) =$ A - $Be^{-k_1 t}$, is shown as a dashed red line, with rate constant k_1 = 0.022 h^1. The $\langle R_H \rangle$ values from microfluidic diffusional sizing are replotted from Paper i. Non-labeled JB6 was diluted from 6 μM to 100 nM. The fit is in the form $\langle R_H \rangle(t) = Ce^{-k_2 t}$ + D, with an apparent dissociation rate constant k_2 = 0.039 h^1 (dashed blue line). The data are displayed with linear and logarithmic time axes in panels A and B, respectively.

Paper iii: Effects of solution conditions on the self-assembly of the chaperone protein DNAJB6b

To understand how JB6 operates at the molecular level, we first need a solid understanding of its intrinsic behavior. Hence, in this paper we undertook a systematic study of JB6's self-assembly under different solution conditions. The main questions addressed were:
1. How does the equilibrium self-assembly distribution of JB6 vary with protein concentration, temperature, pH, ionic strength, and the type of anion along the Hofmeister series?
2. Are monomers or dimers in equilibrium with the micelles?
3. How does the kinetics of micelle dissociation depend on temperature?
4.What insights can be gained by combining results from different techniques that report on distinct biophysical properties — mass, sedimentation coefficient, and hydrodynamic radius?

To measure the self-assembly distribution of JB6, we evaluated and applied the technique of mass photometry, developed in the 2010s [117]. We first verified that JB6 micelles exhibited optical properties similar to those of the globular proteins used to calibrate the mass photometer (Figure 1d in Paper iii), thereby ensuring the reliability of the obtained mass values.

JB6 displays a broad size distribution (Figure 4.6a), with a concentration dependence as shown in Figure 4.6b. The inset illustrates how the average aggregation number, *N*, increases with JB6 concentration.

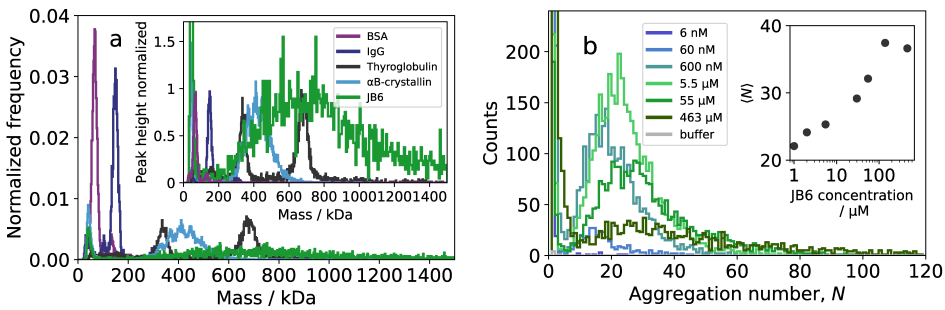

Figure 4.6: Using mass photometry to measure the self-assembly distribution of JB6. **a**: Comparison of the size distributions of known proteins with JB6. **b**: The size distributions of different JB6 concentrations, with the inset showing how the average *N* vary with JB6 concentration.

To determine whether micelles exist in equilibrium with monomers and/or dimers, we explored several approaches. However, due to the low concentration of subunits,

surface activity, and the presence of much larger micelles at $\gtrsim$100 nM, the subunits were difficult to characterize. Here, we extended the calibration curve of the mass photometer below its linear regime by analyzing eight proteins in the 17.4–150 kDa mass range. JB6 have the same mass readout as other monomeric proteins of similar molecular weight (Figure 4.7). No dimeric peak is observed — even at higher concentrations, at 22 or 37 °C, or at pH 7.4 and 150 mM NaCl. We conclude that JB6 is monomeric at concentrations well below its cmc and remains monomeric in equilibrium with micelles at higher concentrations.

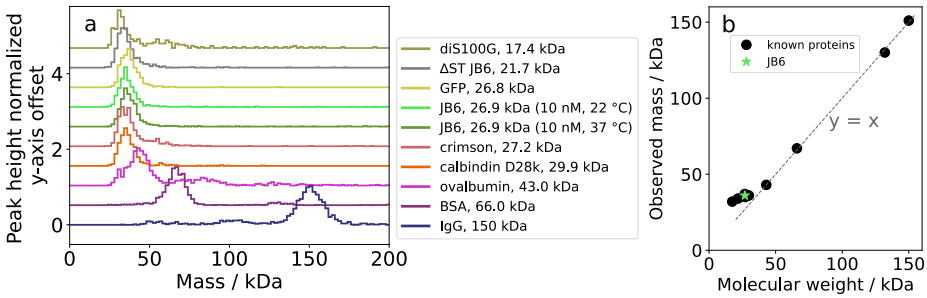

Figure 4.7: Extending the lower limit of mass photometry to examine the JB6 subunit. **a**: Mass distributions of eight proteins with known molecular weights, together with 10 nM pre-equilibrated JB6 at 22 and 37 °C. **b**: The masses from (a) plotted *versus* molecular weight. JB6 aligns with monomeric proteins of ∼26.9 kDa, with no observable dimerization.

In Paper i, the dissociation of JB6 micelles upon dilution at room temperature was probed by measuring $\langle R_H \rangle$ using MDS. Here, we extend this analysis to higher temperatures (22–40 °C), as shown in Figure 4.8a. A strong temperature dependence of the dissociation kinetics is evident, explaining why JB6 exhibit high amyloid-suppression activity also in aggregation kinetics experiments where JB6 had not been pre-incubated at low concentration to allow dissociation, as investigated in Paper ii. The inverse of the dissociation rate constant at 37 °C, $\tau = 1/k$, is approximately 20 min, which explains why a lag phase of about 10 min was required in Paper ii to observe the effect of pre-incubation. In addition to determining JB6 dissociation rates at different temperatures, we calculated the activation energy of the dissociation process using the Arrhenius analysis shown in Figure 4.8b.

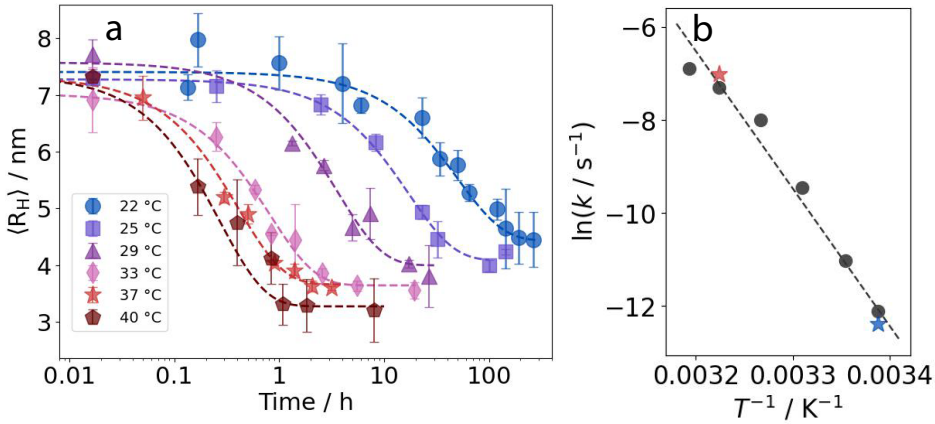

Figure 4.8: **a**: Dissociation of JB6 micelles upon dilution from 5.8 μM to 55 nM, monitored by $\langle R_H \rangle$ obtained using MDS. Single-exponential decay functions ($\langle R_H \rangle(t) = ae^{-kt} + c$) were used to fit the data for each temperature. **b**: Arrhenius plot of the obtained dissociation rate constants from (a) (black circles). Red and blue stars indicate corresponding data obtained by mass photometry. The dashed line represents a fit describing a thermally activated dissociation process, $k_{(T)} = Ae^{-E_a/RT}$, with an activation energy E_a of 250 kJ/mol.

The micelle formation of JB6 has been studied before, both by us and other research groups. But how robust is this process? Is JB6 more or less prone to self-assemble under different solution conditions? By examining self-assembly while varying each parameter across defined intervals, we can learn whether JB6 is likely to self-assemble under physiological conditions, and gain insight into the driving forces of association. Accordingly, we analyzed the self-assembly distribution under different pH values, temperatures, ionic strengths, and anions across the Hofmeister series.

Using analytical ultracentrifugation (AUC) and mass photometry, we detected no difference in micelle size distributions between room temperature and 37 °C. The addition of "salting-in" ions decreased the micelle size, as observed using MDS, AUC, and mass photometry, yet micelles were still formed (Figure 8 in Paper iii).

The largest change in size distribution was observed when varying pH. This was done in the interval pH 2.0-8.0, and between approximately pH 5 and 7, JB6 precipitated, as observed from increased turbidity in light-scattering measurements (Figure 4.9a). Samples of 30 μM JB6 in the pH regions with high JB6 solubility were analyzed by MDS, mass photometry, and AUC, with results shown in Figures 4.9b–d. The size distributions are highly similar at pH 5.0, 7.4, and 8.0, but at pH 4 and below a dramatic shift occurs, evident from both mass photometry and AUC. Micelles at low pH exhibit a narrower distribution and an average $N \approx 10$, compared to ≈ 35 at higher pH values. This change in self-assembly coincides with denaturation of the C-terminal domain (CTD), as observed by circular dichroism (CD) spectroscopy (Figure 6 in Paper iii), consistent with the NTD being more stable [127].

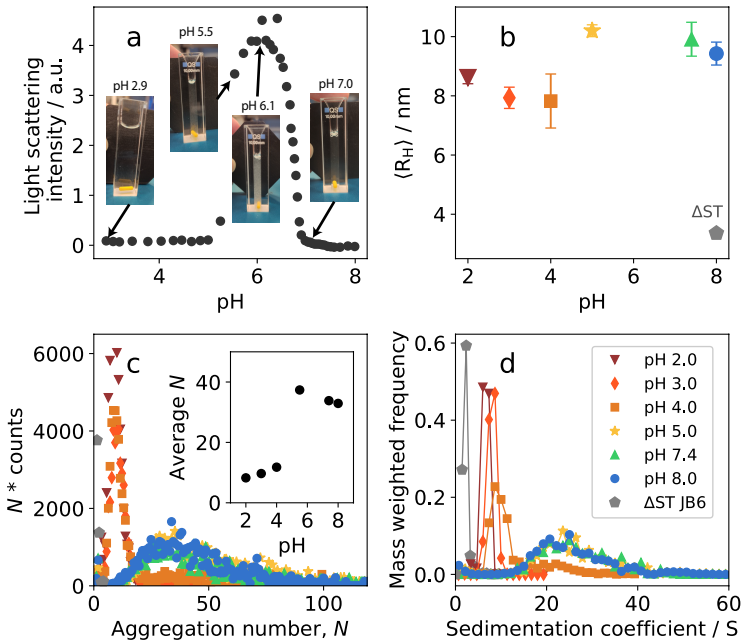

Figure 4.9: Varying pH. **a**: Turbidity measurement upon stepwise addition of 20 mM phosphoric acid to an initial solution of 10 μM JB6, 20 mM NaP, and 0.2 mM EDTA, pH 8.0, at room temperature. **b**: $\langle R_H \rangle$ of JB6 at different pH values, obtained using MDS. **c**: Mass-weighted size distributions of the same JB6 samples as in (b), obtained using mass photometry. The inset shows how the average *N* changes with pH. **d**: Distributions of sedimentation coefficients for the same samples as in (b) and (c), obtained using AUC. The monomeric JB6 variant, ΔST, is included in panels (b–d) for reference. Colors and symbols in the legend are valid for panels (b–d).

Mass photometry reports on particle mass, while AUC reports on sedimentation coefficients, which are connected by the Svedberg equation (Eq. 4.1):

$$S = \frac{m_\mathrm{p} - m_\mathrm{w}}{6\pi\eta R_H} = \frac{V_\mathrm{p}\rho_\mathrm{p} - V_\mathrm{p}\rho_\mathrm{w}}{6\pi\eta R_H} = \frac{m_\mathrm{p}\left(1 - \frac{\rho_\mathrm{w}}{\rho_\mathrm{p}}\right)}{6\pi\eta R_H} \tag{4.1}$$

Here, S is the sedimentation coefficient, m_p the particle (protein) mass, m_w the mass of excluded water, η the solvent viscosity, R_H the hydrodynamic radius, V_p the protein volume, ρ_p the density of pure protein (1.4 g/ml, mean value from [128] and [129]), and ρ_w the density of water (1.0 g/ml). Using this relation, R_H was calculated for each pair of mass and sedimentation coefficient (Figure 7 in Paper iii). The resulting R_H distributions correlated well with the independently measured $\langle R_H \rangle$ from MDS. From the volumes defined by R_H, we calculated particle densities for each mass/sedimentation pair. This analysis show that JB6 micelles are highly solvated, and increasingly so at lower pH — as expected given the higher net charge and more unfolded parts.

Paper iv: Human chaperone DNAJB6b suppresses tau fibril formation through co-aggregation

Considering the close relation between tau aggregation and AD pathology, and given the potency with which JB6 suppresses aggregation of several amyloid-prone clients, surprisingly little has been published about the interplay between these two proteins. However, two studies of cell-lines report that JB6 is crucial for preventing tau aggregation [11, 12]. This further emphasizes the importance of understanding how JB6 may suppress tau aggregation.

Hence, we set out to address the following questions:
1. Does JB6, by itself, influence tau aggregation, and does it affect the kinetics, the equilibrium, or both?
2. In the case of observable effects, which of the microscopic steps in the tau self-assembly mechanism are affected by the presence of JB6?
3. What is the affinity of JB6 for tau fibrils and monomers, respectively?
4. Can we detect the formation of co-aggregates of JB6 with any tau species?

There are several isoforms of tau, and in the body the protein undergoes post-translational modifications (mainly phosphorylation). Consequently, tau aggregation in AD is heterogeneous, and establishing a general aggregation process in *in vitro* studies is not straightforward. Furthermore, full-length tau may have a high nucleation barrier which is sometimes lowered using co-aggregation with negatively charged polyanions for aggregation studies. Here, we use a tau fragment spanning the amyloid core found in AD fibrils (residues 304–380C322S) [58], which has been shown to aggregate rapidly and reproducibly [130], with a solubility in the low nanomolar range [125]. This construct is primarily considered a model system for studying tau aggregation. Nevertheless, it contains the same aggregation-driving segments as the heterogeneous *in vivo* tau population, and core fibrils of this region are present in the body due to their protease resistance [63, 64, 65].

Aggregation kinetics were measured in the presence of different JB6 concentrations (Figure 4.10). The fluorescence of X43 was used as a reporter of fibril mass. JB6 was found to be remarkably potent in prolonging the lag phase of tau aggregation, even at very sub-stoichiometric ratios (a clear inhibition at a 1:700 JB6:tau molar ratio, Figure 4.10a). When the reaction was initiated with 1 % tau seeds, thereby bypassing primary nucleation, JB6 still showed a strong inhibitory effect (Figure 4.10b). At the highest JB6 concentrations, the seeds were rendered completely incompetent, as seen in the lag-time plot (Figure 4.10c). This shows that also secondary growth processes are affected by JB6.

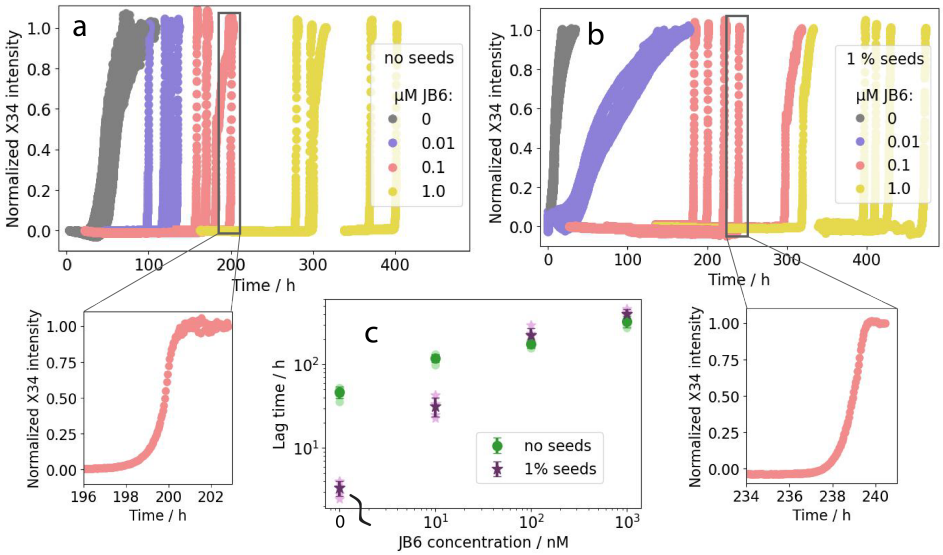

Figure 4.10: Aggregation kinetics of tau in the absence and presence of different JB6 concentrations. **a**: 0 % seeds. **b**: 1 % seeds. Since the lag phase is so long compared to the growth phase, a kinetic trace from each seed condition is shown with expanded x-axis, showing the expected sigmoidal shape. **c**: Lag times (defined as the time at 10 % of the plateau intensity) for the aggregation traces in (a) and (b).

Fits to aggregation kinetics with no and 50 % seeds were used to quantify which microscopic steps are affected by JB6 (Figure 4.11). By varying one rate constant at a time as a function of JB6 concentration, we found that JB6 greatly reduces the rate constant for primary nucleation, as demonstrated by the good fits under non-seeded conditions when varying k_n. The elongation rate constant, k_+, is also decreased by JB6, but only slightly, as concluded from the 50 % seeded condition where elongation strongly dominates the kinetics. The effect on k_2 proved difficult to isolate in a similar manner, as this process is already saturated at tens of nM — consistent with our measurements of tau alone and previous findings [106]. However, cryo-EM images show that JB6 coats the fibril surfaces, and we therefore conclude that k_2 is likely targeted by JB6 as well.

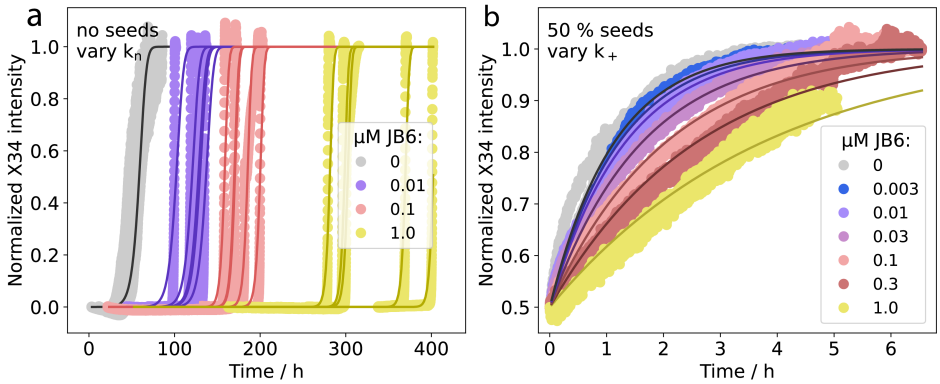

Figure 4.11: Fits of tau aggregation kinetics with 0 and 50 % seeds. Two of three rate constants were kept constant, freely varying the third.

Cryo-EM imaging was performed on tau fibrils, JB6 alone, and samples where tau was allowed to aggregate in the presence of JB6 (Figure 4.12). The fibrils formed with JB6 appear more granular than pure tau fibrils, which we interpret as JB6 co-aggregating with tau.

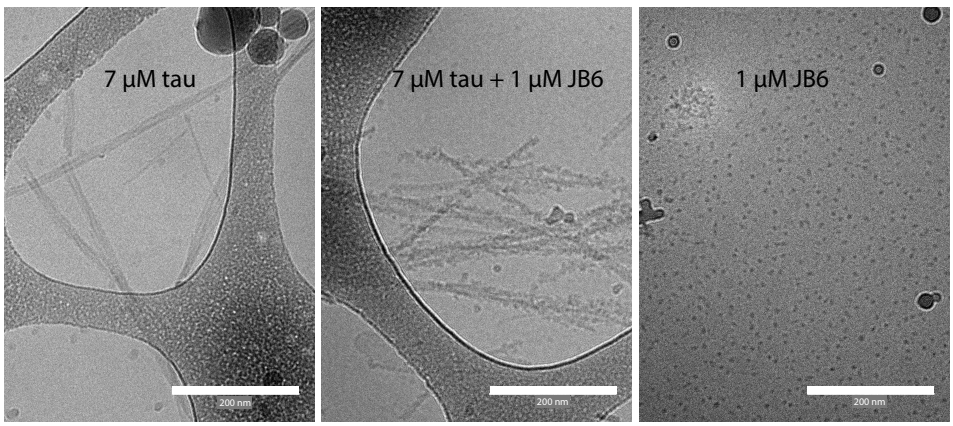

Figure 4.12: Cryo-EM images of tau fibrils, tau+JB6 (monomeric tau let to aggregate in the presence of JB6), and JB6 alone (micelles).

To learn more about the JB6:tau stoichiometry in the fibrils and to assess whether tau solubility is affected, samples withdrawn during aggregation were centrifuged to separate fibrils from material in solution. The supernatant and dissolved pellet were analyzed by reversed-phase HPLC with UV detection to quantify both tau and JB6

(Figure 4.13a). These data show that early pelletable aggregates are rich in JB6 (approximately 1:2 JB6:tau, based on concentration changes between time points). Once JB6 is depleted from solution, tau aggregates rapidly. Interestingly, the apparent solubility of tau (measured after fibril formation) is higher when tau was allowed to co-aggregate with JB6 (Figure 4.13b). This aligns with the hypothesis that JB6 possesses a high chemical potential, which it can reduce by co-aggregating with client proteins. This yields co-aggregates with a higher chemical potential than pure tau fibrils but lowers the overall free energy of the system [110]. Similar behavior has been observed for α-synuclein [104] and Aβ42 [93].

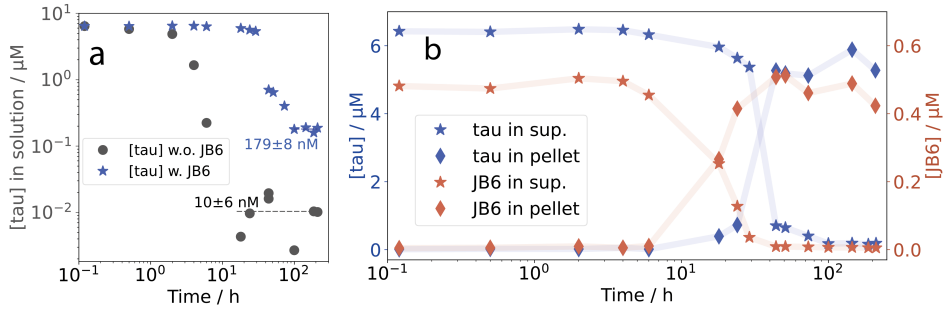

Figure 4.13: Following the amounts of tau and JB6 during the aggregation process, quantified by HPLC with UV absorbance. Centrifugation was used to separate large aggregates from the solution. The initial concentration of monomeric tau was 7 µM. **a**: The concentration of tau during fibril formation, in the absence and presence of 0.7 µM JB6. The values obtained after the aggregation process had ceased were used to calculate the mean and standard deviation of the apparent solubility. **b**: The concentrations of JB6 and tau in the supernatant and dissolved pellet when 0.7 µM JB6 was present from the start of the aggregation process.

We also studied the affinity of JB6 for monomeric and fibrillar tau. Interactions with monomeric tau were investigated using ^{1}H–^{15}N 2D and ^{1}H 1D NMR experiments on ^{15}N-labeled tau, in the absence and presence of a 1:1 molar ratio of non-labeled JB6 (Figure 7 in Paper iv). No interactions were detected. The affinity for tau fibrils was measured by incubating different JB6 concentrations with a constant amount of preformed fibrils, pelleting the fibrils and bound JB6, and quantifying the remaining JB6 in solution by HPLC. Fits to the resulting binding curve yielded a K_D of 200 nM and a saturation stoichiometry of 1.6 JB6 per tau molecule (Figure 6 in Paper iv). Cryo-EM imaging supports the conclusion that JB6 can associate extensively with tau fibrils, fully coating them.

Taken together, these findings show that JB6 by itself potently suppresses tau aggregation, and that it does so via co-aggregation. This represents a pronounced step forward in our understanding of endogenous defense mechanisms against AD. Future studies will focus on identifying the interaction sites of both proteins, which may inspire new therapeutic strategies.

Paper v: The chaperone DNAJB6b halts amyloid formation through association with transient Aβ oligomers

In Paper ii, we asked which aggregation state of JB6 interacts with amyloid peptides. Here, we reverse the question and ask which aggregation state(s) of the amyloid peptides JB6 interacts with. Given the ability of JB6 to prevent amyloid formation at very low sub-stoichiometric chaperone-to-monomer molar ratios, JB6 likely binds to rare and transient amyloid species, such as amyloid oligomers, thereby preventing their growth into mature fibrils. Thus, in this study, we seek to detect such interactions.

Since amyloid oligomers are generally rare and unstable species, we use a model system based on a short amyloid β peptide comprising residues 20–34 (Aβ20–34), which has a high aqueous solubility that enables experiments at millimolar concentrations [131]. JB6 is found to be a potent inhibitor of Aβ20–34 at a highly sub-stoichiometric molar ratio of 1:100,000 chaperone to amyloid peptide (Figure 3a in Paper v). To study the interaction of JB6 with amyloid oligomers, samples withdrawn from ongoing amyloid formation were centrifuged to pellet fibrils, and the supernatant was mixed with fluorescently labeled JB6 (Alexa 488). The average hydrodynamic radius, $\langle R_h \rangle$, of the fluorescent species was measured using MDS. The experimental setup has previously been used to identify amyloid-oligomer binders from an S100G-based library [132].

As shown in Figure 4.14a, the $\langle R_h \rangle$ of JB6 alone and in the presence of monomeric Aβ20–34 is approximately 3 nm. At intermediate times during the fibril formation process, the radius increases, indicating binding between JB6 and amyloid species that are not pelletable. The radius returns to 3 nm as the fibrils mature at the end of the experiment time, indicating that the bounded species appear to have a maximum concentration around halfway during the fibril formation process, $t_{1/2}$. Both these properties of the bounded species: non-pelletable aggregates with a maximum concentration at about $t_{1/2}$, is characteristic for amyloid oligomers [66], prompting us to call the bounded species oligomers.

The same analysis was performed with Aβ42 (Figure 4.14b), yielding a similar result, although with a smaller increase in radius and a longer time before the radius returned to 3 nm. The concentration of Aβ42 oligomers may be lower, and their size smaller, compared to Aβ20–34, making this system more challenging to study. Nevertheless, JB6 appears to bind to Aβ42 oligomers, and we conclude that the interaction of JB6 with amyloid oligomers is not restricted to the short fragment but also applies to the disease-related peptide.

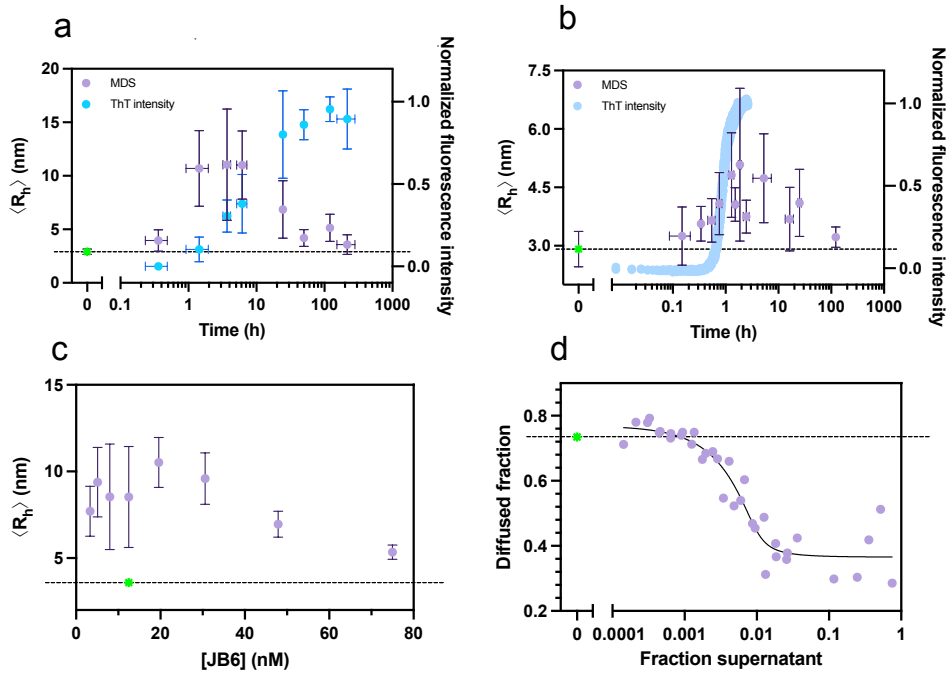

Figure 4.14: Detection of JB6 binding to oligomers. Supernatants from ongoing amyloid formation were mixed with Alexa488-JB6. 6.5 mM Aβ20–34 in **a** and 4 μM Aβ42 in **b**. The $\langle R_h \rangle$ of JB6 mixed with monomeric amyloid peptide is similar to that of JB6 alone (∼3 nm) and is shown in green at time zero. Data are pooled from 3-4 independent experiments, with standard deviations in both x- and y-directions shown as error bars. The ThT intensity of the full sample is shown on the right y-axis. **c**: $\langle R_h \rangle$ of 3–75 nM Alexa488-JB6 mixed with supernatant from aggregating Aβ20-34 (at times of maximal radius, 4.5-5.5 h, diluted 40-fold). **d**: Diffused fraction obtained from MDS for samples with constant JB6 concentration and varying % v/v of Aβ20–34 supernatant at intermediate aggregation times. Data are fitted using an equation for independent binding (Equation 1 in Paper v).

To determine whether the measured $\langle R_h \rangle$ reflects the size of the JB6-amyloid complex — rather than an average of free and bound JB6 — different concentrations of JB6 were added to the supernatant at approximately 5 h into the aggregation process (when the maximum $\langle R_h \rangle$ was observed), shown in Figure 4.14c. At sufficiently low JB6 concentrations, essentially all JB6 molecules are bound, and the measured $\langle R_h \rangle$ therefore represents the size of the complex. Below approximately 30 nM JB6, this condition is fulfilled, and the $\langle R_h \rangle$ of the complex is estimated to be approximately 10 nm.

The affinity of JB6 towards Aβ20–34 oligomers was estimated from samples containing a constant Alexa488-JB6 concentration and varying % v/v of supernatant collected at intermediate aggregation times (2-7 h), when oligomer concentrations are highest. MDS measures the fluorescent intensity in two outlets after the sample have passed a diffusion capillary (see Figure 3.2). The fraction of sample that has diffused to the other half of the channel (the diffused fraction) is used to calculate the $\langle R_h \rangle$.

Since binding models should be applied to quantities closest to the raw experimental data, the diffused fraction was used for fitting (4.14d). The best fit was obtained for $K_D = 1$ nM, indicating an interaction with high affinity.

The interaction between JB6 and Aβ20–34 oligomers was also analyzed in terms of spontaneous dissociation kinetics, where JB6 was found to stabilize the oligomers against dissociation (Figure 4.15). This stabilization may hinder their further growth and conversion into mature amyloids, thereby delaying nucleation and suppressing the autocatalytic generation of additional oligomers through secondary processes. Since amyloid oligomers are believed to play a key role in disease progression [70, 71, 72, 73, 74, 75, 77], binding to these species is of particular interest, and further insight into this mechanism may provide clues to how disease progression can be counteracted.

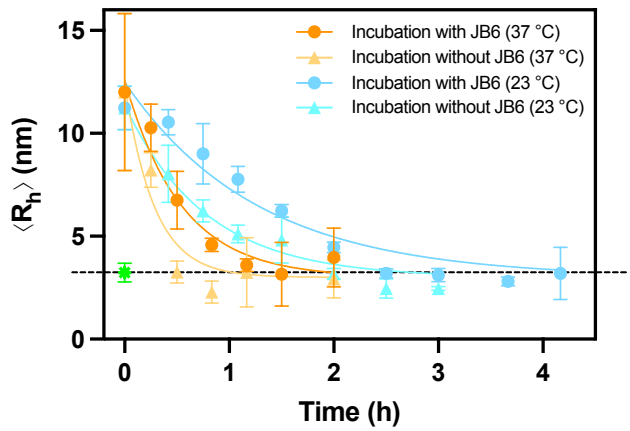

Figure 4.15: Aβ20–34 oligomer size as a function of incubation time at 37 °C and 23 °C. Alexa488-JB6 was added either before (circles) or after (triangles) different incubation times (x-axis) to Aβ20–34 supernatant samples containing oligomers. The $\langle R_h \rangle$ was measured using MDS and plotted as mean values from 3 or 4 replicates, with error bars representing standard deviations. Fits to the data using a single-exponential decay function, $ae^{-kx} + c$, are shown as solid lines.

Chapter 5

Concluding remarks, discussion, and outlook

The long term goal that this thesis work is a part of is to obtain a better understanding of how molecular chaperones, specifically JB6, operates. The most important findings from this thesis are:

- JB6 assembles in a micelle-like manner with a cmc of approximately 120 nM. The micelles exhibit a broad size distribution that is concentration dependent, with an average aggregation number varying between approximately 20 and 40 as the JB6 concentration increases from 1 to 100 μM.
- Monomers are in a dynamic equilibrium with the micelles. At 37 °C, the dissociation from micelles into monomers occur with a half-time of about 20 minutes.
- JB6 is most active in suppressing amyloid formation of Aβ42 in its dissociated state.
- JB6 potently suppresses tau aggregation by co-aggregating at the primary nucleation stage, as well as by binding to mature fibrils.
- JB6 binds strongly to amyloid β oligomers.

Comparative discussion across thesis papers and the literature

In the following, the results and conclusions drawn in this thesis will be compared to findings reported in the literature and with other papers in this thesis.

Regarding the concentration dependence of the self-assembly

In Paper i, the main aim was to study the cmc and micelle dissociation. However, we measured $\langle R_H \rangle$ of up to 100 μM JB6 and observed a flattening of the $\langle R_H \rangle$ increase at high concentrations (Figure 4.1d and Figure 3 in the article), and we concluded at the time that the size did not change notably above approximately 10 μM. Later, in Paper iii, we investigated the micelle size in greater depth and observed a clear size increase in this concentration regime using mass photometry (Figure 4.6b and Figure 1c in the article).

Why was this concentration dependence not apparent in Paper i? First of all, we should examine whether the increase in $\langle R_H \rangle$ above 10 μM can be resolved by MDS. To compare MDS and mass photometry data, the average aggregation number, N, from mass photometry is transformed according to $N^{1/3}$ (scaled by a constant), reflecting the relationship between mass and radius for spherical particles.

$N^{1/3}$, and thus the $\langle R_H \rangle$, is less sensitive to size increases than the mass is, and given the standard deviations in the MDS data as well as the limited number of data points in both series, the MDS data alone are insufficient to conclude that $\langle R_H \rangle$ is constant above approximately 10 μM. In conclusion, we believe that JB6 exhibits concentration-dependent assembly at high concentrations — a conclusion further supported by SAXS, SLS, DLS, and cryo-EM studies — although not distinguishable in the MDS data.

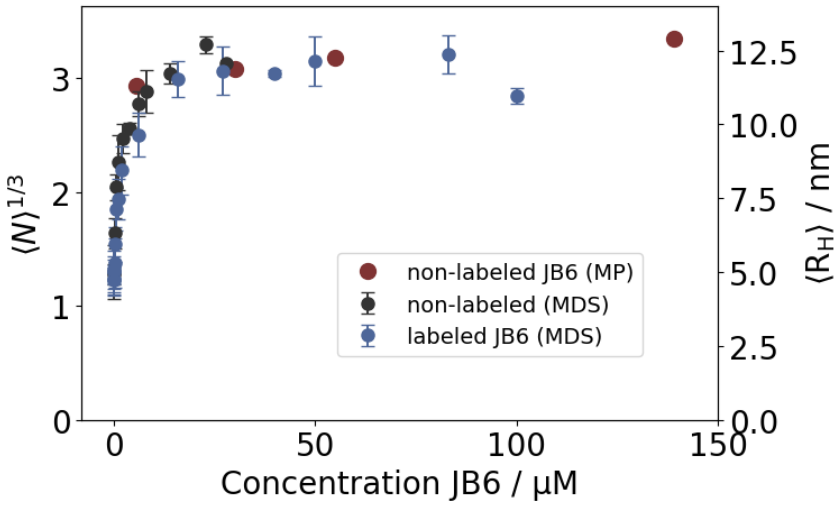

Figure 5.1: Comparison of the concentration dependence of JB6 size, measured by MDS and mass photometry (MP). The N, from mass photometry were transformed with $N^{1/3}$ to facilitate comparison with $\langle R_H \rangle$.

Could the micelles have some low amyloid suppression activity?

In Paper ii, we found that JB6 gains activity upon dissociation into its subunits, but we could not conclude whether the micelles themselves possess any inhibitory activity at all, or not. At the used JB6 concentration of 40 µM, the average aggregation number is approximately 30 (Paper iii, Figure 4.6b), implying that the micelle concentration is roughly 30-fold lower than the monomer concentration. It can therefore not be ruled out that a single micelle has an inhibitory effect comparable to that of a monomer.

However, crosslinked JB6 micelles have been reported to be inactive [99]. To test whether non-crosslinked micelles retain low-level activity, a study analogous to that in Paper ii could be performed at 22 °C, where JB6 dissociates much more slowly than at 37 °C. This would allow the use of higher chaperone concentrations without a rapid increase in monomer concentration following dilution.

About the monomeric subunit of JB6

Some J-domain proteins (JDPs) are known to be dimeric and to function as dimers. JB6 has also previously been suggested to possess a dimeric subunit that assembles into micelles [133]. Consequently, the finding in Paper iii that JB6 exists as monomers in equilibrium with larger micelles, with no detectable dimers, may appear unexpected. However, the study by Söderberg et al. [133] describes an interaction interface be-

tween two JB6 molecules within micelles, rather than isolated subunits existing in equilibrium with the micellar state. Moreover, known dimeric JDPs share a conserved C-terminal dimerization domain. This is the case for class A JDPs and canonical class B JDPs, whereas DNAJB6, DNAJB2, and DNAJB8 lack this region [134]. Figure 5.2a shows a comparison of the domain architecture of class A and class B JDPs. Figure 5.2b illustrates how the dimerization domains of DNAJB1 interact in a crystal structure composed of two copies of the C-terminal half of DNAJB1 [135], PDB: 3AGX. This structure is similar to that reported by Hu et al. [136]. DNAJB1 has further been shown to bind α-synuclein fibrils as a dimeric unit [137].

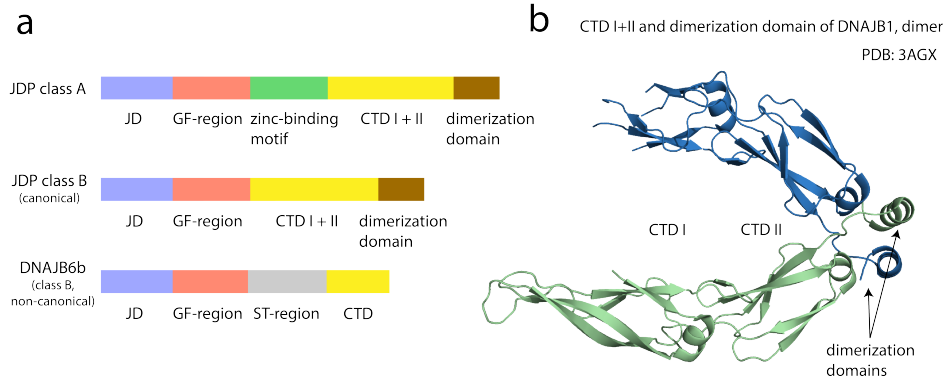

Figure 5.2: **a**: Comparison of class A and canonical class B J-domain proteins. DNAJB6 belongs to the non-canonical class, together with DNAJB2, DNAJB7, and DNAJB8 [134]. **b**: Crystal structure of two C-terminal halves of DNAJB1 associated into a dimeric structure via their dimerization domains [135], which DNAJB6 lacks.

Regarding the tau fragment used as a model system in Paper iv

An important next step will be to extend the tau–JB6 studies to longer tau variants, thereby probing a system more closely resembling the one found in human cells. The large inhibitory effect of JB6 on the tau fragment which is used in this work demonstrates that JB6 has affinity for at least this region of tau. In vivo, tau fibrils undergo enzymatic removal of the fuzzy coat, resulting in fibrils that are more similar to the fragment employed here. The finding of high affinity binding to this region therefore suggests that JB6 may also be active at later stages of disease.

Nevertheless, further studies using longer tau constructs will be necessary to understand how JB6 interacts with additional tau segments. Moreover, phosphomimetic variants and conditions that promote the AD–specific tau fold [138] will be of particular interest in future work, to elucidate how JB6 binds to and affects these disease-relevant tau structures.

Next area of focus: identifying the client-binding region of JB6 — with preliminary results

So far, we have mainly discussed the extent to which JB6 self-assembles and co-assembles with amyloid-forming proteins, and how this behavior affects fibril formation kinetics. The next critical step is to understand *how* JB6 functions as an efficient chaperone at the molecular level. Initial insights into this question were obtained in Paper iii by analyzing JB6 self-assembly under different solution conditions. This led to the conclusion that the propensity to self-assemble is strong and largely governed by the linker region, with both electrostatic and hydrophobic interactions contributing.

However, several key questions remain unresolved. Is the entire linker region equally important for client binding? Is the linker alone sufficient, possibly flanked by suitable solubilizing domains? Or do the folded domains of JB6 themselves directly participate in client recognition? And, importantly, what molecular features of the client protein does JB6 bind to?

These questions will be of high priority in future work, as their answers are central to understanding the binding mechanism of JB6. Such knowledge may also provide inspiration for novel therapeutic strategies, not only for AD but for a broader range of protein aggregation disorders.

A range of experimental methods can be used to identify detailed binding interfaces, including cryo-EM, X-ray crystallography, and NMR spectroscopy in both solid and solution states. We are currently working on structural studies using cryo-EM. However, the lack of symmetry in the complexes, together with difficulties in particle identification and the inherent heterogeneity of client assemblies (including oligomers and fibrils of varying size and morphology), have so far made this a challenging task. Crystallization and solid-state NMR spectroscopy have also been largely unsuccessful. We will continue with further optimization of these approaches. Enrichment of co-oligomers and labeling of the chaperone may provide ways forward. Liquid-state NMR spectroscopy presents additional challenges, as the size, flexibility, and self-assembly behavior of JB6 make it a difficult system to study by this technique. Nevertheless, newly designed monomeric variants of JB6, or constructs containing only parts of the protein, may provide an opportunity for high-quality NMR analysis. Furthermore, if a small, soluble client substrate with an exposed interaction site can be identified, this could enable direct mapping of the JB6 binding interface. However, it is possible that no such substrate exists, as JB6 binding may require energetically frustrated regions or larger assemblies with inherently low solubility.

An alternative strategy has been explored in parallel with the above mentioned approaches. This approach involves designing constructs composed of selected domains

or linker segments of JB6, in some cases fused to other, stable domains, to determine whether specific aspects of chaperone activity can be isolated and attributed to defined sequence elements. While this strategy may provide with lower resolution in terms of the binding site, it may be useful to find out how different segments affect both self-and co-assembly of JB6. We need to be careful in our interpretations since a given sequence may not behave identically outside its native context. Thus, we will combine the chaperone activity measurements with analyses of folding (e.g. using CD spectroscopy) and self-assembly behavior (e.g. using mass photometry). Preliminary results of the amyloid inhibition potential of some designed constructs are summarized below. The architectures of the constructs are shown as AlphaFold3 structure predictions with colored regions in Figure 5.3.

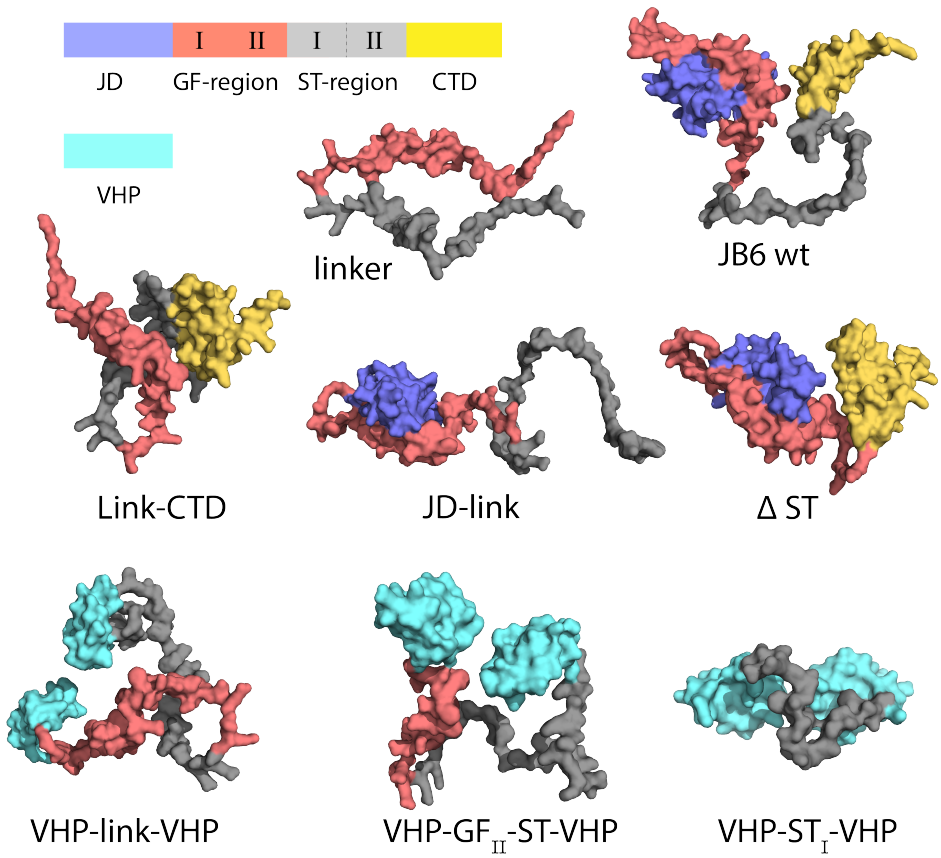

Figure 5.3: AlphaFold3 structure predictions of designed constructs, with color coded regions according to the scheme to the upper left. Illustrated with PyMol, surface representation.

In an initial set of constructs, specific regions of JB6 were deleted, resulting in proteins comprising individual domains (the CTD and J-domain (JD)), the linker alone, or

combinations of domains and linker segments. The ability of these constructs to inhibit Aβ42 aggregation was assessed using ThT fluorescence, with the aggregation half-time, $t_{1/2}$, serving as a first quantitative measure of inhibitory activity (Figure 5.4a).

The JD alone appears neither to possess inhibitory activity, nor to contribute directly to the activity of full-length JB6, as the link-CTD construct exhibits similar activity to the wild-type protein. However, the JD-link, linker alone, and link-CTD constructs are highly aggregation prone, highlighting the role of the folded domains in solubilizing the linker. To perform Aβ42 aggregation kinetics in the presence of self-aggregating constructs, 2-2.5 M urea was used to dissolve them, and prior to the ThT assay they where diluted heavily in buffer, yielding an urea concentration that has insignificant effect on Aβ42 aggregation [139]. The linker itself has already been studied in this way, with similar result as seen in figure 5.3, provided that the assay is run shortly after dilution from urea, since the aggregated linker is inactive [140].

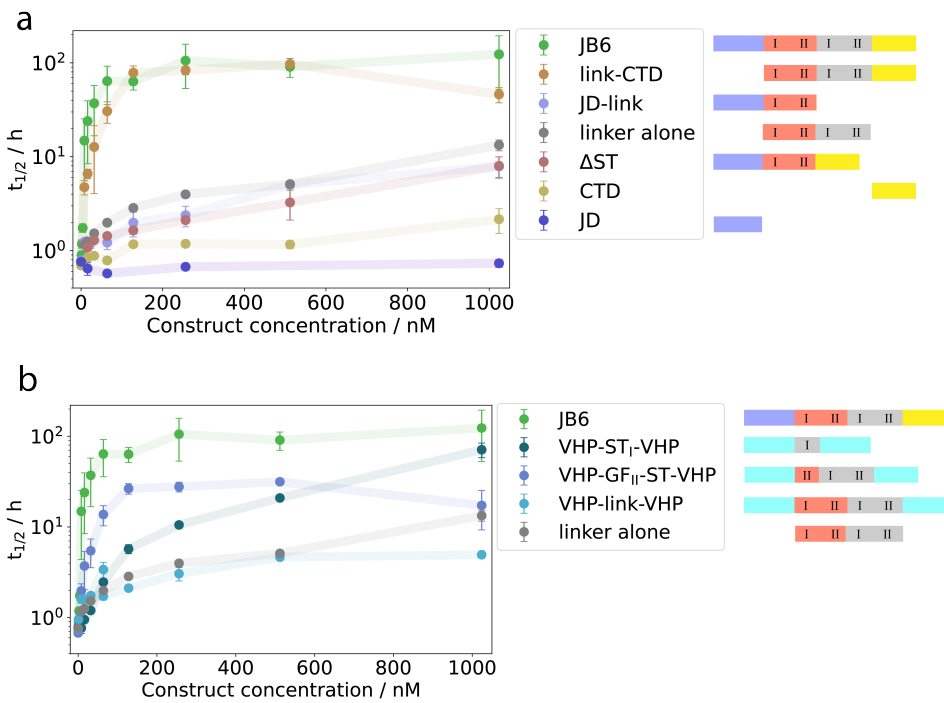

Figure 5.4: Amyloid suppression activity of designed constructs. The $t_{1/2}$ is the time at which 4 μM Aβ42 has reached halfway to the final fibril mass and can be seen as a value of inhibitor activity. The constructs comprise the parts indicated by the color blocks given to the right, which are the same as given in Figure 5.3. **a**: Constructs with different parts of the wt JB6 removed. **b**: The solubility domain villin headpiece (VHP) at each side of different length of the JB6 linker, with wt JB6 and the linker alone as comparisons.

In contrast, the C-terminal domain (CTD) appears to contribute meaningfully to amyloid inhibition. Constructs lacking the CTD display reduced activity compared to wt JB6. While the CTD alone only slightly increases $t_{1/2}$, analysis of aggregation kinetics shows that the CTD reduces the secondary nucleation rate, which has a smaller effect on $t_{1/2}$ than primary nucleation inhibition [94]. It remains unresolved whether the CTD directly participates in client binding and/or enhances the effectiveness of the linker, for instance by promoting solubility or maintaining an unfolded state of the linker that facilitates interaction.

To address the question of which parts of the linker and the CTD are needed for amyloid inhibition, constructs were designed in which different lengths of the linker were flanked by the villin headpiece (VHP), a 35 amino acid long, folded domain that act as a solubilizer with similar net charge as the JD and CTD. These constructs are illustrated as AlphaFold3 structure predictions in Figure 5.3. The construct called VHP-GF_{II}-ST-VHP comprise of the second half of the GF-region, flanked by VHP. This construct was designed in order to shorten the linker but potentially keep the activity, and is motivated by that the first half of the GF-region is found to interact with the JD [91]. Preliminary data indicate that this construct has a higher activity compared to when the whole linker is inserted between two VHPs (VHP-link-VHP). This suggests that the C-terminal part of the linker is more important for client binding. Potentially, the shorter linker is more available for interactions, either due to less internal fold or higher solubility. Still, both VHP-GF_{II}-ST-VHP and VHP-link-VHP aggregates on their own. However, the construct with VHP-ST_I-VHP, where ST_I is the N-terminal half of the ST-region, is soluble and fairly active.

Further analyses of the above constructs, and additional ones, will help determining the specific linker and CTD segments responsible for client binding. Successfully designing monomeric constructs that recapitulate the wild-type activity may also facilitate high-resolution structural studies, such as solution-state NMR, to precisely map the client interaction sites.

In addition to identifying the client binding site, it is of great interest to extend the studies to include how the client binding is coupled to HSP70 activation. Functional assays, such as measuring ATPase activity [91] or monitoring the refolding of heat-denatured luciferase [141], could provide insight into the efficiency and mechanism of HSP70 activation by different JB6 constructs.

Understanding this interplay between JB6, its client, and HSP70 will help to clarify whether specific regions of JB6 not only bind the client but also contribute to chaperone recruitment and activation, potentially revealing mechanistic principles applicable to other J-domain proteins.

Lessons learned from JB6: A recipe for a good molecular chaperone

As a final reflection, it may be valuable to summarize what the studies on JB6 have taught us about the general properties that make a molecular chaperone effective in suppressing protein aggregation of multiple clients. Such a molecule is likely to need:

1. **Exposed hydrophobic regions in a frustrated, partially unfolded state.** These regions provide a high chemical potential due to the ordering of water molecules at the hydrophobic patches, which are freed upon binding to aggregation-prone segments of client proteins. To efficiently suppress primary nucleation, the binding region should be extended, rather than limited to a few amino acids.
2. **Oligomerization.** To prevent the molecule from aberrant self-aggregation — due to its exposed hydrophobic parts — it should self-assemble into finite particles, in contrast to precipitates or amyloids. This allows the chaperone to remain in solution and stay biologically active.
3. **Dynamic exchange between oligomer and monomer.** This ensures that the active monomeric form is available at biologically relevant concentrations, allowing rapid response to client proteins. Solubilizing domains of low net-charge, which flank the unfolded part is a possible way to achieve this.
4. **A functional J-domain for HSP70 activation.** For clients that require ATP-driven mechanisms facilitated by HSP70, such as refolding or degradation, the J-domain must be accessible to HSP70.

The first three criteria relate primarily to the biophysical properties of the chaperone, rather than the exact amino acid sequence. This implies that it should be possible to design new chaperones with sequences different from JB6 that still fulfill these functional requirements. In contrast, to fulfill the last criteria (possessing a J-domain which can activate HSP70), sequence-specificity is important and the particular properties of a few amino acids seems crucial.

References

[1] Jack, C. R. *et al.* Revised criteria for diagnosis and staging of Alzheimer's disease: Alzheimer's Association Workgroup. *Alzheimer's and Dementia* **20**, 5143–5169 (2024).

[2] Verkhratsky, A., Olabarria, M., Noristani, H. N., Yeh, C.-Y. & Rodriguez, J. J. Astrocytes in Alzheimer's Disease. Tech. Rep.

[3] Leng, F. & Edison, P. Neuroinflammation and microglial activation in Alzheimer disease: where do we go from here? (2021).

[4] Hartl, F. U., Bracher, A. & Hayer-Hartl, M. Molecular chaperones in protein folding and proteostasis (2011).

[5] Hipp, M. S., Kasturi, P. & Hartl, F. U. The proteostasis network and its decline in ageing (2019).

[6] 2025 Alzheimer's disease facts and figures. *Alzheimer's & Dementia* **21**, e70235 (2025). URL `https://doi.org/10.1002/alz.70235`.

[7] Hageman, J. *et al.* A DNAJB Chaperone Subfamily with HDAC-Dependent Activities Suppresses Toxic Protein Aggregation. *Molecular Cell* **37**, 355–369 (2010).

[8] Kakkar, V. *et al.* The S/T-Rich Motif in the DNAJB6 Chaperone Delays Polyglutamine Aggregation and the Onset of Disease in a Mouse Model. *Molecular Cell* **62**, 272–283 (2016).

[9] Månsson, C. *et al.* DNAJB6 is a peptide-binding chaperone which can suppress amyloid fibrillation of polyglutamine peptides at substoichiometric molar ratios. *Cell Stress and Chaperones* **19**, 227–239 (2014).

[10] Månsson, C. *et al.* Interaction of the molecular chaperone DNAJB6 with growing amyloid-beta 42 (Aβ42) aggregates leads to sub-stoichiometric inhibition of amyloid formation. *Journal of Biological Chemistry* **289**, 31066–31076 (2014).

[11] Esquivel, A. R., Hill, S. E. & Blair, L. J. DnaJs are enriched in tau regulators. *International Journal of Biological Macromolecules* **253** (2023).

[12] Chang, Y. L. *et al.* The HSP40 family chaperone isoform DNAJB6b prevents neuronal cells from tau aggregation. *BMC Biology* **21** (2023).

[13] Kuriyan, J., Konforti, B. & Wemmer, D. *The MOLECULES of LIFE Physical and Chemical Principles*.

[14] Dill, K. A. Dominant Forces in Protein Folding (1990). URL `https://pubs.acs.org/sharingguidelines`.

[15] O'Neil, K. & DeGrado, W. A Thermodynamic Scale for the Helix-Forming Tendencies of the Commonly Occurring Amino Acids. *Science* **250**, 646–651 (1990).

[16] Minor, D. & Kim, P. Measurement of the beta-sheet-forming propensities of amino acids. *Nature* **367** (1994).

[17] Dunker, A. K., Silman, I., Uversky, V. N. & Sussman, J. L. Function and structure of inherently disordered proteins (2008).

[18] Holehouse, A. S. & Kragelund, B. B. The molecular basis for cellular function of intrinsically disordered protein regions (2024).

[19] Jumper, J. *et al.* Highly accurate protein structure prediction with AlphaFold. *Nature* **596**, 583–589 (2021).

[20] Mirdita, M. *et al.* ColabFold: making protein folding accessible to all. *Nature Methods* **19**, 679–682 (2022).

[21] Nick Pace, C., Martin Scholtz, J. & Grimsley, G. R. Forces stabilizing proteins (2014).

[22] Israelachvili, J. *Intermolecular and Surface Forces* (Academic Press, 2011), third edition edn.

[23] Evans, F., D. & Wennerström, H. *The Colloidal Domain: Where Physics, Chemistry, Biology, and Technology Meet* (John Wiley Sons Inc, 1999), 1 edn.

[24] Hubbard, R. E. & Kamran Haider, M. Hydrogen Bonds in Proteins: Role and Strength. In *Encyclopedia of Life Sciences* (Wiley, 2010).

[25] Bosshard, H. R., Marti, D. N. & Jelesarov, I. Protein stabilization by salt bridges: Concepts, experimental approaches and clarification of some misunderstandings (2004).

[26] Langmuir, I. THE CONSTITUTION AND FUNDAMENTAL PROPERTIES OF SOLIDS AND LIQUIDS I SOLIDS. *Journal of the American Chemical Society* **11**, 2221–2295 (1916). URL https://pubs.acs.org/sharingguidelines.

[27] Henry, E. R. *et al.* Allosteric control of hemoglobin S fiber formation by oxygen and its relation to the pathophysiology of sickle cell disease. *Proceedings of the National Academy of Sciences* **117**, 15018–15027 (2020). URL https://www.pnas.org/doi/abs/10.1073/pnas.1922004117.

[28] Sheng, J., Olrichs, N. K., Gadella, B. M., Kaloyanova, D. V. & Bernd Helms, J. Regulation of functional protein aggregation by multiple factors: Implications for the amyloidogenic behavior of the cap superfamily proteins (2020).

[29] Maji, S. K. *et al.* Functional Amyloids As Natural Storage of Peptide Hormones in Pituitary Secretory Granules. *Science* **325**, 328–332 (2009). URL https://doi.org/10.1126/science.1173155.

[30] Jang, H. *et al.* Antimicrobial Protegrin-1 Forms Amyloid-Like Fibrils with Rapid Kinetics Suggesting a Functional Link. *Biophysical Journal* **100**, 1775–1783 (2011). URL https://www.sciencedirect.com/science/article/pii/S0006349511002426.

[31] Roan, N. R. *et al.* Semen amyloids participate in spermatozoa selection and clearance. *eLife* **6**, e24888 (2017). URL https://doi.org/10.7554/eLife.24888.

[32] Nagaraj, M. *et al.* Chaperones mainly suppress primary nucleation during formation of functional amyloid required for bacterial biofilm formation. *Chemical Science* **13**, 536–553 (2022).

[33] Yu, B. *et al.* Assembly and recognition of keratins: A structural perspective. *Seminars in Cell and Developmental Biology* **128**, 80–89 (2022).

[34] IUPAC Compendium of Chemical Terminology. oligomer molecule (2025). URL https://doi.org/10.1351/goldbook.O04286.

[35] Carlsson, A., Olsson, U. & Linse, S. On the micelle formation of DNAJB6b. *QRB Discovery* **4** (2023).

[36] IUPAC Compendium of Chemical Terminology. micelle (2025). URL https://doi.org/10.1351/goldbook.M03889.

[37] Augusteyn, R. C. & Koretz, J. F. A possible structure for α-crystallin. *FEBS Letters* **222**, 1–5 (1987).

[38] De Kruif, C. G. Supra-aggregates of Casein Micelles as a Prelude to Coagulation. *Journal of Dairy Science* **81**, 3019–3028 (1998).

[39] Nichols, E. *et al.* Estimation of the global prevalence of dementia in 2019 and forecasted prevalence in 2050: an analysis for the Global Burden of Disease Study 2019. *The Lancet Public Health* **7**, e105–e125 (2022).

[40] Seshadri, S. & Wolf, P. A. Lifetime risk of stroke and dementia: current concepts, and estimates from the Framingham Study. *The Lancet Neurology* **6**, 1106–1114 (2007). URL https://doi.org/10.1016/S1474-4422(07)70291-0.

[41] Alzheimer, A. Über eine eigenartige Erkrankung der Hirnrinde. *Allg Z Psych Psychgerich Med* **64**, 146–148 (1907).

[42] Stelzmann, R. A., Norman Schnitzlein, H. & Reed Murtagh, F. An english translation of alzheimer's 1907 paper, "über eine eigenartige erkankung der hirnrinde". *Clinical Anatomy* **8**, 429–431 (1995).

[43] Glenner, G. G. & Wong, C. W. Alzheimer's disease: initial report of the purification and characterization of a novel cerebrovascular amyloid protein. *Biochemical and Biophysical Research Communications* **120**, 885–890 (1984).

[44] Hardy, J. A. & Higgins, G. A. Alzheimer's Disease: The Amyloid Cascade Hypothesis. *Science* **256**, 184–185 (1992). URL https://doi.org/10.1126/science.1566067.

[45] Selkoe, D. J. The Molecular Pathology of Alzheimer's Disease. Tech. Rep. (1991).

[46] Hansson, O. Biomarkers for neurodegenerative diseases (2021).

[47] Findeis, M. A. The role of amyloid β peptide 42 in Alzheimer's disease (2007).

[48] Haass, C. *et al.* The Swedish mutation causes early-onset Alzheimer's disease by β-secretase cleavage within the secretory pathway. *Nature Medicine* **1**, 1291–1296 (1995). URL https://doi.org/10.1038/nm1295-1291.

[49] H, v. D. C. *et al.* Lecanemab in Early Alzheimer's Disease. *New England Journal of Medicine* **388**, 9–21 (2023). URL https://doi.org/10.1056/NEJMoa2212948.

[50] Sims, J. R. *et al.* Donanemab in Early Symptomatic Alzheimer Disease: The TRAILBLAZER-ALZ 2 Randomized Clinical Trial. *JAMA* **330**, 512–527 (2023).

[51] Buxbaum, J. N. *et al.* Amyloid nomenclature 2024: update, novel proteins, and recommendations by the International Society of Amyloidosis (ISA) Nomenclature Committee. *Amyloid* **31**, 249–256 (2024).

[52] Rambaran, R. N. & Serpell, L. C. Amyloid fibrils. *Prion* **2** (2008).

[53] Welander, H. *et al.* Aβ43 is more frequent than Aβ40 in amyloid plaque cores from Alzheimer disease brains. *Journal of Neurochemistry* **110**, 697–706 (2009).

[54] Yang, Y. *et al.* Cryo-EM structures of amyloid-β 42 filaments from human brains. *Science* **375**, 167–172 (2022). URL `https://doi.org/10.1126/science.abm7285`.

[55] Goedert, M., Wischik, C. M., Crowther, R. A., Walker, J. E. & Klug, A. Cloning and sequencing of the cDNA encoding a core protein of the paired helical filament of Alzheimer disease: Identification as the microtubule-associated protein tau (molecular pathology/neurodegenerative disease/neurofibriliary tangles). Tech. Rep. (1988).

[56] Goedert, M., Spillantini, M. C., Lakes, R., Rutherford, D. & Crowther, R. A. Multiple lsoforms of Human Microtubule-Associated Protein Tau: Sequences and localization in Neurofibrillah Tangles of Alzheimer's Disease. Tech. Rep. (1989).

[57] Weingarten, M. D., Lockwood, A. H., Hwo, S.-Y. & Kirschner, M. W. A Protein Factor Essential for Microtubule Assembly. *Proceedings of the National Academy of Sciences of the United States of America* **72**, 1858–1862 (1975). URL `https://www.pnas.org`.

[58] Fitzpatrick, A. W. *et al.* Cryo-EM structures of tau filaments from Alzheimer's disease. *Nature* **547**, 185–190 (2017).

[59] Goedert, M., Spillantini, M. G., Cairns, N. J. & Crowther, R. A. Tau Proteins of Alzheimer Paired Helical Filaments: Abnormal Phosphorylation of All Six Brain lsoforms I. Tech. Rep. (1992).

[60] Grundke-Iqbal, I. *et al.* Abnormal phosphorylation of the microtubule-associated protein X (tau) in Alzheimer cytoskeletal pathology (Alzheimer disease/neurofibrillary tangles/paired-helical filaments/microtubules). Tech. Rep. (1986).

[61] Mandelkow, E.-m. *et al.* Tau Domains, Phosphorylation, and Interactions With Microtubules. Tech. Rep. 95 (1995).

[62] Hanger, D. P., Anderton, B. H. & Noble, W. Tau phosphorylation: the therapeutic challenge for neurodegenerative disease (2009).

[63] Wischik, C. M. *et al.* Structural characterization of the core of the paired helical filament of Alzheimer disease (molecular pathology/neurodegenerative disease/neurofibrillary tangles/snnng transmission electron microscopy). Tech. Rep. (1988).

[64] Novak, M., Kabat, J. & Wischikl, C. M. Molecular characterization of the minimal protease resistant tau unit of the Alzheimer's disease paired helical filament. Tech. Rep. 1 (1993).

[65] Moloney, C. M., Lowe, V. J. & Murray, M. E. Visualization of neurofibrillary tangle maturity in Alzheimer's disease: A clinicopathologic perspective for biomarker research (2021).

[66] Michaels, T. C. *et al.* Dynamics of oligomer populations formed during the aggregation of Alzheimer's Aβ42 peptide. *Nature Chemistry* **12**, 445–451 (2020).

[67] Arosio, P., Knowles, T. P. & Linse, S. On the lag phase in amyloid fibril formation. *Physical Chemistry Chemical Physics* **17**, 7606–7618 (2015).

[68] Cohen, S. I., Vendruscolo, M., Dobson, C. M. & Knowles, T. P. From macroscopic measurements to microscopic mechanisms of protein aggregation (2012).

[69] Meisl, G. *et al.* Molecular mechanisms of protein aggregation from global fitting of kinetic models. *Nature Protocols* **11**, 252–272 (2016).

[70] Cohen, S. I. *et al.* A molecular chaperone breaks the catalytic cycle that generates toxic Aβ oligomers. *Nature Structural and Molecular Biology* **22**, 207–213 (2015).

[71] Oda, T. *et al.* Clusterin (apoJ) Alters the Aggregation of Amyloid β-Peptide (Aβ1-42) and Forms Slowly Sedimenting Aβ Complexes That Cause Oxidative Stress. *Experimental Neurology* **136**, 22–31 (1995). URL `https://www.sciencedirect.com/science/article/pii/S0014488685710801`.

[72] Walsh, D. M. & Selkoe, D. J. Aβ oligomers - A decade of discovery (2007).

[73] Walsh, D. M. *et al.* Naturally secreted oligomers of amyloid b protein potently inhibit hippocampal long-term potentiation in vivo. Tech. Rep. (2002). URL `www.nature.com`.

[74] Sakono, M. & Zako, T. Amyloid oligomers: Formation and toxicity of Aβ oligomers (2010).

[75] Haass, C. & Selkoe, D. J. Soluble protein oligomers in neurodegeneration: Lessons from the Alzheimer's amyloid β-peptide (2007).

[76] Flagmeier, P. *et al.* Direct measurement of lipid membrane disruption connects kinetics and toxicity of Aβ42 aggregation. *Nature Structural and Molecular Biology* **27**, 886–891 (2020).

[77] Otzen, D. E. Antibodies and α-synuclein: What to target against Parkinson's Disease? *Biochimica et Biophysica Acta - Proteins and Proteomics* **1872** (2024).

[78] Meisl, G. *et al.* Uncovering the universality of self-replication in protein aggregation and its link to disease. Tech. Rep. (2022). URL `https://www.science.org`.

[79] Ellis, R. J. Ellis 1987 Molecular Chaperones. *Nature* (1987).

[80] Ellis, R. Ellis 2001 Cell crowding .

[81] Finka, A. & Goloubinoff, P. Proteomic data from human cell cultures refine mechanisms of chaperone-mediated protein homeostasis. *Cell Stress and Chaperones* **18**, 591–605 (2013).

[82] Kampinga, H. H. *et al.* Function, evolution, and structure of J-domain proteins (2019).

[83] Kampinga, H. H. *et al.* Guidelines for the nomenclature of the human heat shock proteins (2009).

[84] Liu, Q., Liang, C. & Zhou, L. Structural and functional analysis of the Hsp70/Hsp40 chaperone system (2020).

[85] Rosenzweig, R., Nillegoda, N. B., Mayer, M. P. & Bukau, B. The Hsp70 chaperone network (2019).

[86] Mauthe, M. *et al.* A chaperone-proteasome-based fragmentation machinery is essential for aggrephagy. *Nature Cell Biology* (2025).

[87] Zhang, R., Malinverni, D., Cyr, D. M., Rios, P. D. L. & Nillegoda, N. B. J-domain protein chaperone circuits in proteostasis and disease (2023).

[88] Hanai, R. & Mashima, K. Characterization of two isoforms of a human DnaJ homologue, HSJ2. Tech. Rep. (2003).

[89] Thiruvalluvan, A. *et al.* DNAJB6, a Key Factor in Neuronal Sensitivity to Amyloidogenesis. *Molecular Cell* **78**, 346–358 (2020).

[90] Karamanos, T. K., Tugarinov, V. & Clore, G. M. Unraveling the structure and dynamics of the human DNAJB6b chaperone by NMR reveals insights into Hsp40-mediated proteostasis. *Proceedings of the National Academy of Sciences of the United States of America* **116**, 21529–21538 (2019).

[91] Abayev-Avraham, M., Salzberg, Y., Gliksberg, D., Oren-Suissa, M. & Rosenzweig, R. DNAJB6 mutants display toxic gain of function through unregulated interaction with Hsp70 chaperones. *Nature Communications* **14** (2023).

[92] Hobbs, B. *et al.* A low-complexity linker as a driver of intra- and intermolecular interactions in DNAJB chaperones. *Nature Communications* **16** (2025).

[93] Månsson, C. *et al.* Conserved S/T Residues of the Human Chaperone DNAJB6 Are Required for Effective Inhibition of Aβ42 Amyloid Fibril Formation. *Biochemistry* **57**, 4891–4892 (2018).

[94] Österlund, N. *et al.* The C-terminal domain of the antiamyloid chaperone DNAJB6 binds to amyloid-β peptide fibrils and inhibits secondary nucleation. *Journal of Biological Chemistry* **299** (2023).

[95] Kuiper, E. F. *et al.* The chaperone DNAJB6 surveils FG-nucleoporins and is required for interphase nuclear pore complex biogenesis. *Nature Cell Biology* **24**, 1584–1594 (2022).

[96] Watson, E. D., Geary-Joo, C., Hughes, M. & Cross, J. C. The Mrj co-chaperon mediates keratin turnover and prevents the formation of toxic inclusion bodies in trophoblast cells of the placenta. *Development* **134**, 1809–1817 (2007).

[97] Ruggieri, A. *et al.* DNAJB6 myopathies: Focused review on an emerging and expanding group of myopathies (2016).

[98] Sarparanta, J. *et al.* Mutations affecting the cytoplasmic functions of the co-chaperone DNAJB6 cause limb-girdle muscular dystrophy. *Nature Genetics* **44**, 450–455 (2012).

[99] Österlund, N., Lundqvist, M., Ilag, L. L., Gräslund, A. & Emanuelsson, C. Amyloid-β oligomers are captured by the DNAJB6 chaperone: Direct detection of interactions that can prevent primary nucleation. *Journal of Biological Chemistry* **295**, 8135–8144 (2020).

[100] Carlsson, A., Axell, E., Emanuelsson, C., Olsson, U. & Linse, S. The Ability of DNAJB6b to Suppress Amyloid Formation Depends on the Chaperone Aggregation State. *ACS Chemical Neuroscience* **15**, 1732–1737 (2024).

[101] Aprile, F. A. *et al.* The molecular chaperones DNAJB6 and Hsp70 cooperate to suppress α-synuclein aggregation. *Scientific Reports* 7 (2017).

[102] Arkan, S., Ljungberg, M., Kirik, D. & Hansen, C. DNAJB6 suppresses alpha-synuclein induced pathology in an animal model of Parkinson's disease. *Neurobiology of Disease* **158** (2021).

[103] Deshayes, N., Arkan, S. & Hansen, C. The molecular chaperone DNAJB6, but Not DNAJB1, suppresses the seeded aggregation of alpha-synuclein in cells. *International Journal of Molecular Sciences* **20** (2019).

[104] Pálmadóttir, T. *et al.* The Role of α-Synuclein–DNAJB6b Coaggregation in Amyloid Suppression. *ACS Chemical Neuroscience* (2025).

[105] Gillis, J. *et al.* The DNAJB6 and DNAJB8 protein chaperones prevent intracellular aggregation of polyglutamine peptides. *Journal of Biological Chemistry* **288**, 17225–17237 (2013).

[106] Rodríguez-González, C., Lin, S., Arkan, S. & Hansen, C. Co-chaperones DNAJA1 and DNAJB6 are critical for regulation of polyglutamine aggregation. *Scientific Reports* **10** (2020).

[107] Chien, V. *et al.* The chaperone proteins HSP70, HSP40/DnaJ and GRP78/BiP suppress misfolding and formation of β-sheet-containing aggregates by human amylin: A potential role for defective chaperone biology in Type 2 diabetes. *Biochemical Journal* **432**, 113–121 (2010).

[108] Udan-Johns, M. *et al.* Prion-like nuclear aggregation of TDP-43 during heat shock is regulated by HSP40/70 chaperones. *Human Molecular Genetics* **23**, 157–170 (2014).

[109] Carlsson, A. *et al.* Effects of solution conditions on the self-assembly of the chaperone protein DNAJB6b. *Communications Chemistry* **8**, 289 (2025). URL `https://www.nature.com/articles/s42004-025-01697-7`.

[110] Linse, S., Thalberg, K. & Knowles, T. P. The unhappy chaperone. *QRB Discovery* **2** (2021).

[111] Williams, T. L. & Serpell, L. C. Membrane and surface interactions of Alzheimer's Aβ peptide - Insights into the mechanism of cytotoxicity. In *FEBS Journal*, vol. 278, 3905–3917 (2011).

[112] Jones, E. M. *et al.* Interaction of Tau Protein with Model Lipid Membranes Induces Tau Structural Compaction and Membrane Disruption. *Biochemistry* **51**, 2539–2550 (2012). URL `https://doi.org/10.1021/bi201857v`.

[113] Pallbo, J., Fornasier, M., Linse, S. & Olsson, U. Air–Water Interfacial Adsorption of the Chaperone Protein DNAJB6b. *Langmuir* **41**, 19146–19155 (2025).

[114] Yates, E. V. *et al.* Latent analysis of unmodified biomolecules and their complexes in solution with attomole detection sensitivity. *Nature Chemistry* **7**, 802–809 (2015).

[115] Zhang, Y. *et al.* On-chip measurements of protein unfolding from direct observations of micron-scale diffusion. *Chemical Science* **9**, 3503–3507 (2018).

[116] Cole, D., Young, G., Weigel, A., Sebesta, A. & Kukura, P. Label-Free Single-Molecule Imaging with Numerical-Aperture-Shaped Interferometric Scattering Microscopy. *ACS Photonics* **4**, 211–216 (2017).

[117] Young, G. *et al.* Quantitative mass imaging of single biological macromolecules. *Science* 423–427 (2018).

[118] Wu, D. & Piszczek, G. Standard protocol for mass photometry experiments. *European Biophysics Journal* **50**, 403–409 (2021).

[119] Demeler, B. Methods for the design and analysis of sedimentation velocity and sedimentation equilibrium experiments with proteins. *Current Protocols in Protein Science* (2010).

[120] Levine, H. Thioflavine T interaction with synthetic Alzheimer's disease beta-amyloid peptides: Detection of amyloid aggregation in solution. *Protein Science* **2**, 404–410 (1993).

[121] Biancalana, M. & Koide, S. Molecular mechanism of Thioflavin-T binding to amyloid fibrils (2010).

[122] Lindberg, D. J., Wranne, M. S., Gilbert Gatty, M., Westerlund, F. & Esbjörner, E. K. Steady-state and time-resolved Thioflavin-T fluorescence can report on morphological differences in amyloid fibrils formed by Aβ(1-40) and Aβ(1-42). *Biochemical and Biophysical Research Communications* **458**, 418–423 (2015).

[123] Zhang, J. *et al.* Detection and Imaging of Aβ1-42 and Tau Fibrils by Redesigned Fluorescent X-34 Analogues. *Chemistry - A European Journal* **24**, 7210–7216 (2018).

[124] Styren, S. D., Hamilton, R. L., Styren, G. C. & Klunk, W. E. X-34, A Fluorescent Derivative of Congo Red: A Novel Histochemical Stain for Alzheimer's Disease Pathology. Tech. Rep. 9 (2000). URL `http://www.jhc.org`.

[125] Axell, E. *et al.* Solubility and Metastability of the Amyloidogenic Core of Tau. *ACS Chemical Neuroscience* (2026). URL https://pubs.acs.org/doi/10.1021/acschemneuro.5c00784.

[126] Johansson, B. Agarose gel electrophoresis. *Scandinavian Journal of Clinical and Laboratory Investigation* **29**, 7–19 (1972).

[127] Fricke, C. *et al.* On the thermal and chemical stability of DNAJB6b and its globular domains. *Biophysical Chemistry* **320-321**, 107401 (2025).

[128] Cantor R., C. & Schimmel R., P. *Biophysical Chemistry Part II: Techniques for the study of biological structure and function* (W. H. Freeman and Company, San Francisco, 1980).

[129] Van Holde, K. E., Johnson, W. C. & Ho, P. S. *Principles of physical biochemistry* (Pearson/Prentice Hall, 1998).

[130] Rodriguez Camargo, D. C. *et al.* Proliferation of Tau 304-380 Fragment Aggregates through Autocatalytic Secondary Nucleation. *ACS Chemical Neuroscience* **12**, 4406–4415 (2021).

[131] Warmack, R. A. *et al.* Structure of amyloid-β (20-34) with Alzheimer's-associated isomerization at Asp23 reveals a distinct protofilament interface. *Nature Communications* **10** (2019).

[132] Linse, S., Sormanni, P. & O'connell, D. J. An aggregation inhibitor specific to oligomeric intermediates of Aβ42 derived from phage display libraries of stable, small proteins (2022). URL https://doi.org/10.1073/pnas.2121966119.

[133] Söderberg, C. A. *et al.* Structural modelling of the DNAJB6 oligomeric chaperone shows a peptide-binding cleft lined with conserved S/T-residues at the dimer interface. *Scientific Reports* **8** (2018).

[134] Kirstein, J. *et al.* J-domain proteins: from molecular mechanisms to diseases. *Cell Stress and Chaperones* 100142 (2025). URL https://linkinghub.elsevier.com/retrieve/pii/S1355814525000872.

[135] Suzuki, H. *et al.* Peptide-Binding Sites As Revealed by the Crystal Structures of the Human Hsp40 Hdj1 C-Terminal Domain in Complex with the Octapeptide from Human Hsp70. *Biochemistry* **49**, 8577–8584 (2010). URL https://doi.org/10.1021/bi100876n.

[136] Hu, J. *et al.* The crystal structure of the putative peptide-binding fragment from the human Hsp40 protein Hdj1. *BMC Structural Biology* **8** (2008).

[137] Monistrol, J. *et al.* Stepwise recruitment of chaperone Hsc70 by DNAJB1 produces ordered arrays primed for bursts of amyloid fibril disassembly. *Communications Biology* **8**, 522 (2025).

[138] Lövestam, S. *et al.* Assembly of recombinant tau into filaments identical to those of Alzheimer's disease and chronic traumatic encephalopathy. *eLife* **11** (2022).

[139] Weiffert, T. *et al.* Influence of denaturants on amyloid β42 aggregation kinetics. *Frontiers in Neuroscience* **16** (2022).

[140] Merkelis, T., Olsson, U. & Linse, S. The low complexity linker of DNAJB6b is key to its anti-amyloid function. *QRB Discovery* **6** (2025).

[141] Ayala Mariscal, S. M. *et al.* Identification of a HTT-specific binding motif in DNAJB1 essential for suppression and disaggregation of HTT. *Nature Communications* **13** (2022).

Printed by Media-Tryck, Lund 2026 NORDIC SWAN ECOLABEL 3041 0903

About the author

Andreas Carlsson pursued a Master of Science in Engineering in Technical Nanoscience at Lund University, driven by a long-standing curiosity about the fundamental principles governing the material world. He found protein science to be a perfect match, as it naturally bridges chemistry, physics, biology, medicine, and mathematics. After completing his master's thesis in the laboratory of Sara Linse, he continued there as a doctoral researcher. His work focuses on molecular mechanisms involved in the cellular defense against neurodegenerative disorders, with particular emphasis on the chaperone DNAJB6, its self-assembly, and its interactions with amyloidogenic proteins.

LUND UNIVERSITY

Faculty of Science
Biochemistry and Structural Biology

ISBN 978-91-8104-834-6